The zCOSMOS 10k-sample: the role of galaxy stellar mass in the colour-density relation up to z ~ 1

A&A 524, A2 (2010)
DOI: 10.1051/0004-6361/200912585

Astronomy & Astrophysics

The zCOSMOS 10k-sample⋆: the role of galaxy stellar mass in the colour-density relation up to $z \sim 1$

O. Cucciati[1,2], A. Iovino[2], K. Kovač[3], M. Scodeggio[4], S. J. Lilly[3], M. Bolzonella[5], S. Bardelli[5], D. Vergani[5], L. A. M. Tasca[1,4], E. Zucca[5], G. Zamorani[5], L. Pozzetti[5], C. Knobel[3], P. Oesch[3], F. Lamareille[6], K. Caputi[3], P. Kampczyk[3], L. Tresse[1], C. Maier[3], C. M. Carollo[3], T. Contini[6], J.-P. Kneib[1], O. Le Fèvre[1], V. Mainieri[7], A. Renzini[8], A. Bongiorno[9], G. Coppa[5,10], S. de la Torre[1,11,4], L. de Ravel[1], P. Franzetti[4], B. Garilli[4], J.-F. Le Borgne[6], V. Le Brun[1], M. Mignoli[5], R. Pellò[6], Y. Peng[3], E. Perez-Montero[6,12], E. Ricciardelli[13], J. D. Silverman[3], M. Tanaka[7], A. M. Koekemoer[14], N. Scoville[15], U. Abbas[1,16], D. Bottini[4], A. Cappi[5], P. Cassata[1,17], A. Cimatti[10], L. Guzzo[11], A. Leauthaud[18], D. Maccagni[4], C. Marinoni[19], H. J. McCracken[20], P. Memeo[4], B. Meneux[9,21], C. Porciani[22], and R. Scaramella[23]

(Affiliations can be found after the references)

Received 27 May 2009 / Accepted 3 August 2010

ABSTRACT

Aims. With the first ∼10 000 spectra of the flux limited zCOSMOS sample ($I_{AB} \leq 22.5$) we want to study the evolution of environmental effects on galaxy properties since $z \sim 1.0$, and to disentangle the dependence among galaxy colour, stellar mass and local density.

Methods. We use our previously derived 3D local density contrast δ, computed with the 5th nearest neighbour approach, to study the evolution with z of the environmental effects on galaxy U-B colour, D4000 Å break and [OII]λ3727 equivalent width (EW[OII]). We also analyze the implications due to the use of different galaxy selections, using luminosity or stellar mass, and we disentangle the relations among colour, stellar mass and δ studying the colour-density relation in narrow mass bins.

Results. We confirm that within a luminosity-limited sample ($M_B \leq -20.5 - z$) the fraction of red ($U - B \geq 1$) galaxies depends on δ at least up to $z \sim 1$, with red galaxies residing mainly in high densities. This trend becomes weaker for increasing redshifts, and it is mirrored by the behaviour of the fraction of galaxies with D4000 Å break ≥1.4. We also find that up to $z \sim 1$ the fraction of galaxies with $\log(EW[\mathrm{OII}]) \geq 1.15$ is higher for lower δ, and also this dependence weakens for increasing z. Given the triple dependence among galaxy colours, stellar mass and δ, the colour-δ relation that we find in the luminosity-selected sample can be due to the broad range of stellar masses embedded in the sample. Thus, we study the colour-δ relation in narrow mass bins within mass complete subsamples, defining red galaxies with a colour threshold roughly parallel to the red sequence in the colour-mass plane. We find that once mass is fixed the colour-δ relation is globally flat up to $z \sim 1$ for galaxies with $\log(M/M_\odot) \gtrsim 10.7$. This means that for these masses any colour-δ relation found within a luminosity-selected sample is the result of the combined colour-mass and mass-δ relations. On the contrary, even at fixed mass we observe that within $0.1 \leq z \leq 0.5$ the fraction of red galaxies with $\log(M/M_\odot) \lesssim 10.7$ depends on δ. For these mass and redshift ranges, environment affects directly also galaxy colours.

Conclusions. We suggest a scenario in which the colour depends primarily on stellar mass, but for an intermediate mass regime ($10.2 \lesssim \log(M/M_\odot) \lesssim 10.7$) the local density modulates this dependence. These relatively low mass galaxies formed more recently, in an epoch when more evolved structures were already in place, and their longer SFH allowed environment-driven physical processes to operate during longer periods of time.

Key words. galaxies: evolution – galaxies: fundamental parameters – galaxies: statistics – galaxies: high-redshift – cosmology: observations – large-scale structure of Universe

1. Introduction

Galaxies can be considered the building blocks of the universe, and nevertheless we are far from a complete understanding of their formation and evolution. Although theoretical scenarios can help us to address these open issues, only through observations we can robustly shape a coherent picture, following backward galaxy lifetimes from what we see in the local universe up to their undisclosed origins.

The first observations of nearby galaxies led to their morphological classification (Hubble 1926, but see also Sandage 1975). In more recent years, several internal physical galaxy properties have been used in order to classify galaxies. The inter-correlations and scaling laws that were found among these properties and also with morphology (to give only a few examples, the "Fundamental Plane", Djorgovski & Davis 1987; Dressler et al. 1987; the "Photometric Cube", Scodeggio et al. 2002; the colour-magnitude relation, Visvanathan & Sandage 1977; Tully et al. 1982; Gavazzi et al. 1996) have been confirmed in the last years using the data provided by large local galaxy surveys like the Sloan Digital Sky Survey (SDSS, York et al. 2000) and the Two degree Field Galaxy Redshift Survey (2dFGRS, Colless et al. 2001), with the studies by Kauffmann et al. (2004), Baldry et al. (2004), Balogh et al. (2004) and several others. These findings suggested a broad bimodal galaxy classification: 1) the red, passive galaxies, with elliptical/spheroidal shapes and composed by an old (on the mean) population of stars, moving mostly on disordered radial orbits; 2) the blue, active

⋆ European Southern Observatory (ESO), Large Program 175.A-0839.

galaxies, disk-dominated, where stars (of relatively young age) are concentrated in circular orbits.

The close relationship between these galaxy types and local environment was primarily uncovered via the study of nearby clusters. The so-called morphology-density relation, as first quantified by Oemler (1974) and Dressler (1980), holds that star-forming, disk-dominated galaxies tend to reside in regions of lower galaxy density, such as cluster outskirts and the field, while red, elliptical galaxies are found preferentially in the higher density regions, like cluster cores. Recent work based on the 2dFGRS and the SDSS has established that the connections between local environment and morphology holds not only in clusters, but extend continuously over the full range of local densities, from the centers of clusters out into the field population. Moreover, not only morphology, but several other galaxy properties correlate with environment. On average, high density regions are populated mostly by redder, brighter and less star forming galaxies, while the opposite is true for the low density environment (e.g. Balogh et al. 2004; Kauffmann et al. 2004; Tanaka et al. 2004; Blanton et al. 2005; Hogg et al. 2004). These studies also indicated that colour is the property most tightly related to environment.

With the recent advent of large deep galaxy surveys, it has been found that the galaxy bimodal distribution is not characteristic of the local universe only. On the one side, early type galaxies are found to be the predominant population among red and luminous galaxies at all redshift up to $z \sim 1.3$ (see e.g. Bell et al. 2004; Menanteau et al. 2006). On the other side, it has been observed that the bimodal colour distribution holds even up to $z \sim 2$, although with a significant contribution of dusty star forming galaxies to the red population (e.g., Willmer et al. 2006; Franzetti et al. 2007).

Also the environment has been shown to extend its influence on galaxy properties at these high redshifts. In the last decade studies of increasingly distant clusters (to $z \sim 1$) have grown in number, thanks to high-resolution imaging and spectroscopic data. These works have shown, for example, that the fraction of early type galaxies decreases from the inner part of clusters to their outskirts (e.g., Treu et al. 2003), and the fraction of star forming galaxies is higher in the field than in any other environment (e.g., Poggianti et al. 2006). Moreover, it has been shown that, at least up to $z \sim 1$, the fraction of blue galaxies anti-correlates with group richness (Iovino et al. 2010; Cucciati et al. 2010), while the fraction of early-type galaxies correlates with it (Kovač et al. 2010b). Still, comparisons of local results with studies of high-redshift clusters have pointed towards significant evolution in the relationship between galaxy properties and local environment from $z \sim 1$ to the present. For example, the morphology-density relation for galaxies in clusters and groups evolves strongly with increasing redshift (Dressler et al. 1997), and there is evidence that the evolution in intermediate density environments has occurred more recently than in high density environments (Smith et al. 2005). It also appears that the morphological mix of cluster early type galaxies (the relative fraction of lenticular and elliptical galaxies) has changed with time (Fasano et al. 2000; Postman et al. 2005).

Nevertheless, with these high redshift cluster studies it is possible to divide galaxies only into broad environment classifications (such as field, group and cluster populations). Furthermore, clusters include only a relatively small fraction (by number and an even smaller one by volume) of the total galaxy population at any epoch, and therefore they offer only a limited vision on galaxy evolution. The new generation of large and deep redshift surveys very recently allowed us to extend to high redshift the investigation of environmental effects on several galaxy properties within the full range of local densities, from voids and very low densities up to the higher density peaks in the center of clusters. These high redshift studies could help us resolve the still open debate about the origin of environmental effects on galaxy properties. The question is whether these properties were imprinted upon the galaxy population at their formation epoch (the so called "nature" hypothesis), or whether they are a result of environment-driven evolution, i.e. the end products of processes that have operated over a Hubble time (the so called "nurture" scenario).

Many physical mechanisms that could be responsible for this correlation between galaxy properties and environment have been proposed, but up to now there is no a clear understanding of their real role on the observed trends. From preliminary studies of local density and group membership at $z \sim 1$ that have been developed independently and nearly at the same time in these past few years by the VIMOS-VLT Deep Survey (VVDS, Le Fèvre et al. 2005) and by the DEEP2 Galaxy Redshift Survey (Davis et al. 2003), it seems at least that both a biased galaxy formation (galaxies formed earlier in high matter-density peaks, giving galaxies different imprinting of initial conditions, Marinoni et al. 2005) and a complex evolution of star formation quenching (for example the weakening of the colour-density relation at higher redshift, Cucciati et al. 2006 and Cooper et al. 2007, with possibly its reversal at $z \sim 1.5$, Cucciati et al. 2006, but see also Elbaz et al. 2007 and Cooper et al. 2008) concurred to build up the observed relations between environment and galaxy properties. We will discuss more deeply high redshift results in the following of this paper.

A detailed view of the environmental effects on galaxy properties is still missing, however. The scale length at which environment affects the most galaxy properties has been studied in the local universe, and it seems that local density acts on colour, $H\alpha$ equivalent width and D4000 Å break on a scale of $\sim$1 Mpc h^{-1} (Kauffmann et al. 2004, but also Blanton et al. 2006 for scales also $\sim$0.5 Mpc h^{-1}), and what it is observed on larger scales is only a mirror of what really happens on smaller distances. Nevertheless, these results are related only intuitively at the typical scales of cluster halos, and a precise quantification of these observed effects has still to be done. Moreover, as it is known that several properties are inter-related and they also are related with environment, one would like to understand whether the local density affects only a property, that then drives the dependence of the others, or more than one. For example, we already know that mass is responsible for shaping galaxy star formation history (Gavazzi & Scodeggio 1996; Scodeggio et al. 2002; Kauffmann et al. 2003), and moreover mass does depend on environment, as it as been shown at both local and high ($z \sim 1$) redshift (Kauffmann et al. 2004; Bundy et al. 2006; Scodeggio et al. 2009; Bolzonella et al. 2010). Should we consider the galaxy stellar mass as the only property directly affected by the environment, this meaning that the other properties depend on local density only through their dependence on mass? The answer seems not to be unique, as at $z \sim 0.1$ the galaxy colour, D4000 Å break and sSFR are found to depend on environment even when mass is fixed (Kauffmann et al. 2004; Baldry et al. 2006), but no colour-density relation has been found in the range $0.2 \leq z \leq 1.4$ in mass bins within VVDS data (Scodeggio et al. 2009).

In this frame of open issues, we use the first $\sim$10 000 zCOSMOS spectra to inspect more deeply the environmental effects up to $z \sim 1$. With its pure flux limit ($I_{AB} < 22.5$) and small

redshift measurement error ($\sim$100 km s^{-1}), this galaxy sample allowed us to reliably reconstruct the local density field on small scales up to $z \sim 1$, as described in Kovač et al. (2010a). Moreover the quality of the spectra and the multi-wavelength coverage provide us with high quality measurement of several galaxy properties. The paper is organized as follows. In Sects. 2 and 3 we describe the galaxy sample, the galaxy properties we are interested in, how the density contrast has been measured and all the advantages and drawbacks of this measurement. In Sect. 4 we study the redshift evolution of the colour-density relation, together with the dependence on environment of other galaxy properties (D4000 Å break, [OII]λ3727 equivalent width). In Sect. 5 we show how stellar mass depends on local density, and in Sect. 6 we disentangle the correlation among colour, stellar mass and environment. Finally in 7 we discuss the scale dependence of environmental effects. Sections 8–10 are devoted to the discussion of our results and to the conclusions. Throughout this paper we use the cosmological parameters $\Omega_m = 0.25$, $\Omega_\Lambda = 0.75$, $H_0 = 70$ km s^{-1} Mpc^{-1} and $H_0 = 100\,h$. Magnitudes are expressed in the AB system, and absolute magnitudes have $H_0 = 70$ incorporated. Moreover, "mass" always means "stellar mass", unless differently stated.

Parallel analyses about galaxy properties and environment have been carried out within the same data set in other works. Using the density field presented in Kovač et al. (2010a), Bolzonella et al. (2010) and Zucca et al. (2009) study the Galaxy Mass Function and Galaxy Luminosity Function as a function of environment, Tasca et al. (2009) show how the local density affects galaxy morphology and finally Caputi et al. (2009) and Silverman et al. (2009a) study the environment surrounding specific populations (24 μm galaxies and AGN respectively). Moreover, exploiting the group catalog presented in Knobel et al. (2009), Iovino et al. (2010) and Kovač et al. (2010b) study galaxy colour and morphology for group and isolated galaxies. Finally, Peng et al. (2010) draw a global picture on the role of mass and environment in influencing galaxy evolution.

2. DATA

2.1. The zCOSMOS "10k-sample"

zCOSMOS (Lilly et al. 2007) is an on-going large spectroscopic survey, conceived with the main goal of studying high-redshift galaxy environments from very small scales (galaxy groups scales) up to larger-scale structures. Two main projects are part of the zCOSMOS survey: a *bright* survey, aimed to measure spectroscopic redshifts for $\sim$20 000 galaxies with $I_{AB} \leq 22.5$ in the $\sim$1.7 deg^2 COSMOS field (Scoville et al. 2007b), and a *deep* survey, with the goal of acquiring $\sim$10 000 spectra for a sample of colour-selected galaxies residing in the redshift range $1.4 < z < 3.0$, in the central 1 deg^2 of the COSMOS field. The results described in this paper are based on the first $\sim$10 000 measured spectra in the *bright* sample (Lilly et al. 2009). From now on, we will call this sample "10k-sample".

Details about the zCOSMOS survey can be found in Lilly et al. (2007) and Lilly et al. (2009). In summary, spectra have been collected with the VIMOS (Le Fèvre et al. 2003) multi-spectrograph, at ESO Very Large Telescope. *Bright* sample observations have been performed using the Red Medium-Resolution grism ($R \sim 600$, spectral range 5550–9650 Å). The final *bright* sample of $\sim$20 000 will have an estimated sampling rate of $\sim$60–70% homogeneous over almost the entire field, while the 10k-sample has a less homogeneous and lower sampling rate, on average of $\sim$33%, and it actually covers an area of $\sim$1.4 deg^2.

For the data reduction we refer the reader to Lilly et al. (2009). Here it is worth noticing that thanks to repeated observations carried out on a subsample of galaxies, a measurement redshift error of $\sim$100 km s^{-1} has been estimated. For this paper, a subsample of galaxies with an overall 98.4% reliability rate in the redshift measurement have been used. This leave us with a sample of $\sim$7800 galaxies in the redshift range $0.1 \leq z \leq 1.0$.

Finally, the COSMOS field has been covered by multi-wavelength imaging. Optical and Near-IR data are described in Capak et al. (2007). See references therein for details on observations in other wavelengths (XMM-Newton, GALEX, VLA) and Koekemoer et al. (2007) for the HST ACS imaging data.

2.2. Galaxy properties

In this paper we analyze environmental effects on galaxy properties such as absolute magnitude, stellar mass and spectral indexes.

Rest frame absolute magnitudes have been computed from the best fitting template normalized to each galaxy photometry and redshift, using the code *ZEBRA* (Feldmann et al. 2006). The template set is composed by six observed galaxy spectra (four from Coleman et al. 1980 and two from Kinney et al. 1996). We refer the reader to Oesch et al. (2010) for more details. We tested the robustness of our results using also absolute magnitudes derived with the method described in Ilbert et al. (2005), and with two different template sets: the library from Bruzual & Charlot (2003), hereafter BC03, and stellar population models generated using the PEGASE2 population synthesis code (Fioc & Rocca-Volmerange 1997). We obtained consistent results, within error bars, for different choices of template set and/or code.

Galaxy stellar masses have been computed using a SED fitting technique, with the *Hyperzmass* code (a modified version of *Hyperz*, see Bolzonella et al. 2000). Different SED libraries have been used: the widely-used BC03 library, the Maraston (2005, hereafter M05) library and Charlot & Bruzual (2007, hereafter CB07, priv. comm.) library. The imposed Star Formation Histories are 10 exponentially declining SFH with e-folding times from 0.1 to 30 Gyr, plus a model of constant star formation. In this paper we use masses derived with BC03 libraries, a Chabrier Initial Mass Function (Chabrier 2003), and dust extinction modeled with the Calzetti's law (Calzetti et al. 2000). For further details and comparisons among different libraries see Pozzetti et al. (2010). It is worth noticing that results obtained in this paper regarding stellar masses are robust using masses derived with different libraries.

In this work me make use of two spectral features: the equivalent width of the [OII]λ3727 doublet (EW[OII] from now on) and the amplitude of the 4000 Å break in its narrow definition (D_n4000 from now on), as introduced by Balogh et al. (1999). These are computed by an adapted version of the *platefit* code (Lamareille et al. 2006; see also Tremonti et al. 2004; Brinchmann et al. 2004, for the original pipeline). This code fits the stellar continuum and absorption lines making use of the STELIB library (Le Borgne et al. 2003) of stellar spectra and of the GALAXEV (Bruzual & Charlot 2003) stellar population synthesis models. We eliminate from our sample spectral measurements affected either by large uncertainties in the wavelength calibration, by the superposition with strong night sky lines or by stellar continuum subtraction problems. Finally, we consider only spectral line measurements with a line significance (ratio of the maximum flux of a line to the rms of the

continuum around it) higher than 1.15. This threshold allows us to exclude ∼85% of fake detections, and still to include the majority of real emission lines measurements.

For D_n4000 and [OII]λ3727 related measurements, we consider for our analysis the redshift range $0.48 \leq z \leq 1.0$, as the [OII]λ3727 line enters in the spectral range of the adopted grism only at $z = 0.48$ (the D4000 Å break enters at a relatively smaller z, but we want to consider the same z range for the two indicators). In this redshift range, D_n4000 has been reliably computed for ∼4000 galaxies, and we have a successful measurement of [OII]λ3727 equivalent width for ∼2500 galaxies.

2.3. Density

The detailed description of the environment parametrization within the zCOSMOS 10k-sample is given in Kovač et al. (2010a). Here we give only a general overview.

The environment surrounding a given galaxy at comoving position $\boldsymbol{r}$ has been characterized by the dimensionless density contrast $\delta(\boldsymbol{r}) = [\rho(\boldsymbol{r}) - \rho_{\rm m}(\boldsymbol{r})]/\rho_{\rm m}(\boldsymbol{r})$, where density is smoothed with a given filter. In this formula, $\rho_{\rm m}(\boldsymbol{r})$ is the mean density at the redshift that corresponds to the comoving position $\boldsymbol{r}$, while $\rho(\boldsymbol{r})$ is the local density around the given galaxy.

We remark that for the environment parametrization not only the 10k-sample galaxies has been used, but also the remaining ∼30 000 galaxies in the full zCOSMOS photometric catalogue, exploiting their photometric redshifts. Moreover, boundary corrections have been applied to density estimates, to take into account the fact that for galaxies that reside too close to the field edges the filter window will fall out of the survey field. Finally, the robustness of this density reconstruction scheme has been tested with simulated galaxy catalogues.

We refer the reader to Kovač et al. (2010a) for an overview of the properties of the density field reconstructed in the zCOSMOS field. In particular, their Figs. 22–24 show a direct comparison of the density field and the distribution of galaxy groups (Finoguenov et al. 2007; Knobel et al. 2009). Another analysis of the large scale structures in the same field is shown in Scoville et al. (2007a). For example, they remark that the supermassive structure at $z \sim 0.74$ seems to be equivalent, in terms of mass, to the Coma cluster.

Given the lower and less homogeneous sampling rate near the field boundaries, in this work we limit ourselves to the central area of the zCOSMOS field, enclosed within the rectangular area with vertices $ra_{\rm min} = 149.55$, $ra_{\rm max} = 150.42$, $dec_{\rm min} = 1.75$, $dec_{\rm max} = 2.7$.

2.4. Choosing the more suitable density computation approach

The local density $\rho(\boldsymbol{r})$ has been computed with a variety of methods, including different filters, different tracer galaxy populations and different weighting schemes for the tracer galaxies. While Kovač et al. (2010a) discuss all these possibilities, we discuss here only the optimal choice adopted for this work.

The different methods used to estimate the density field produce environment parametrizations with significantly different statistical properties (for example the measurement error, or the homogeneity across the redshift range explored), and it is important to choose the density estimator best suited for any specific scientific analysis.

For our study, we decided to give priority to the density computed on as small a scale as possible. Tests performed using mock catalogues (Kovač et al. 2010a) have shown that with the zCOSMOS 10k-sample we can safely reconstruct the galaxy local environment up to $z \sim 1$ using cylindrical filters with half depth of 1000 km/s, and either a fixed radius $R \geq 3\ h^{-1}$ Mpc, or a variable radius equal to the projected distance of at least the 5th nearest neighbour ("n.n." from now on). As one can see in Fig. 6 of Kovač et al. (2010a), at least at the highest densities the distance D to the 5th n.n. is always smaller than $3\ h^{-1}$ Mpc. Thus we will use the density computed with the 5th n.n. approach. However with this method the scale R varies as a function of environment, being larger for lower densities. This has to be taken into account in the interpretation of our results.

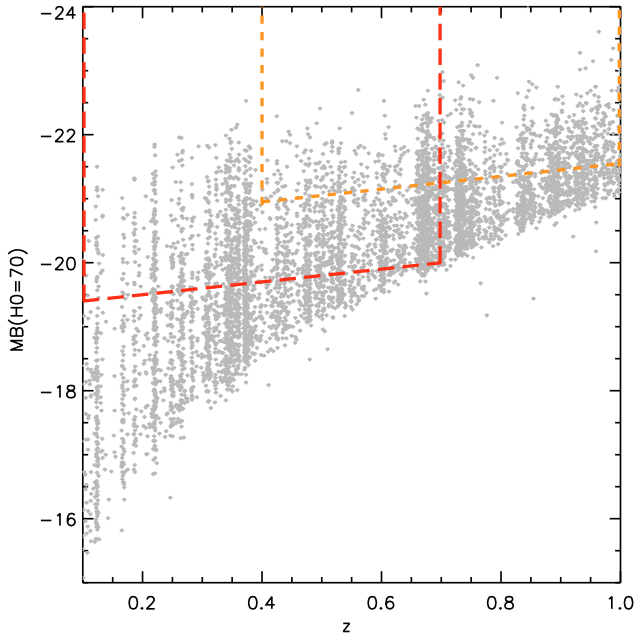

Fig. 1. B-band rest frame absolute magnitudes as a function of redshift for galaxies of the 10k-sample residing in the central area of the zCOSMOS field, in the redshift range considered in this paper. Two time-evolving luminosity volume limits are shown with dashed lines: the red long-dashed line represents the fainter limit ($M_B = -19.3 - z$), for which we are complete up to $z = 0.7$, and the orange short-dashed line is the limit $M_B = -20.5 - z$, for which we are complete up to $z = 1.0$ but for which we have enough galaxies only for $z \geq 0.4$.

Moreover, different tracer galaxy populations have been used for the density computation: the entire flux limited sample ($I_{\rm AB} \leq 22.5$) and two different luminosity-selected volume-limited subsamples, that satisfy the criteria $M_B \leq -19.3 - z$ and $M_B \leq -20.5 - z$. The redshift dependence in these equations has been chosen to take into account the effects of an average passive evolution that should include the majority of galaxy types, and the intercepts values have been chosen in order to define two complete samples at $z = 0.7$ and $z = 1.0$, respectively (Kovač et al. 2010a). This is clearly shown in Fig. 1. The figure shows the B-band absolute magnitude distribution as a function of redshift for the 10k-sample, in the redshift range considered in this paper. The two time-evolving luminosity limits are plotted as dashed lines. From the figure, it is evident that the fainter subsample is defined to inlcude all the objects at its higher redshift ($z = 0.7$), while the brighter subsample at $z = 1$ remains about 0.5 mag brighter than the faintest galaxies that we can see in the 10k-sample. This is due to the fact that our survey is flux-limited in I-band, which corresponds to the restframe B-band at

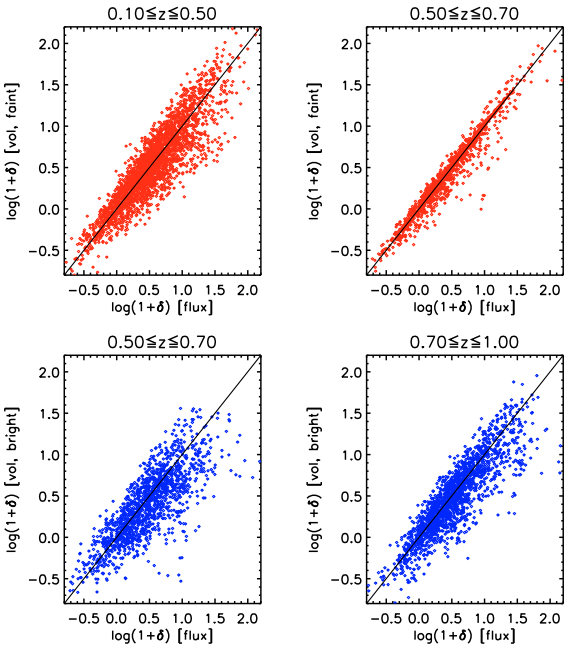

Fig. 2. Comparison of local density computed with volume limited tracers ("vol", y axis) and flux limited tracers ("flux", x axis). The density computed with the faint and bright volume limited tracers is shown in *the top and bottom panels*, respectively, in each case for two redshift bins as indicated on the top of each plot.

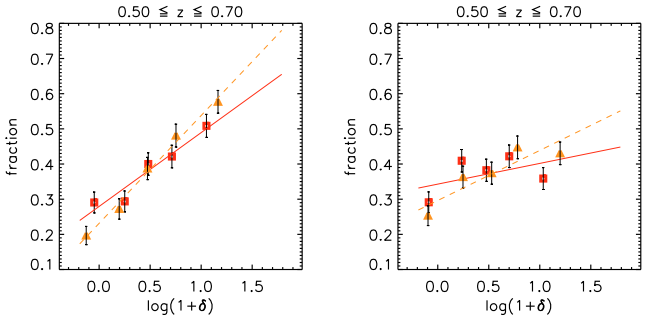

Fig. 3. *Left panel*. Fraction of red ($U - B > 1.0$) galaxies as a function of the density contrast, in equipopulated density bins, for a luminosity-selected volume-limited sample with $M_B \leq -19.3 - z$ in the redshift range $0.5 \leq z \leq 0.7$. Density is computed with the 5th nearest neighbour method, using volume limited tracers ($M_B \leq -19.3 - z$). The values on the x axis represent the median density values in each density bin. Red squares are for density based on counts ("CWD", see text), while orange triangles for density weighted by stellar mass ("MWD"). Vertical error bars are computed applying the binomial formula. Solid line is the linear fit of squares, dashed line the linear fit of triangles. The slopes of the fits with their errors are quoted in the text. *Right panel*. As in the left panel, but in this case, before computing the MWD to each galaxy it has been assigned the entire set of properties (mass, colour etc.) of another galaxy near in redshift, chosen randomly. This way galaxy positions and redshift are not correlated with galaxy properties. See the text for further details.

$z \sim 0.7$. Thus, our sample is complete in restframe B-band at this redshift. At higher redshift, because of the different evolution of different galaxy populations, we start missing the early type galaxies at the faintest B-band magnitudes we can reach. The brighter magnitude limit that we used ensures us to be complete for all galaxy populations.

The advantage in using the flux limited tracers is that we can exploit our entire data set, and we can measure the density contrast down to the smallest scales adopting the 5th n.n. method. There are two drawbacks in using these tracers: the tracer population is not uniform with redshift, as it becomes brighter for higher z, and the mean distance to the 5th n.n. increases with z. Both these issues have to be considered when interpreting any evolutionary environmental effect on galaxy properties. These disadvantages are not present if we use a luminosity-selected volume-limited sample of tracers. For these reasons, we decided to use the density contrast computed with the tracers limited at $M_B \leq -19.3 - z$ or $M_B \leq -20.5 - z$, according to the redshift range we want to explore. The limit at $M_B \leq -20.5 - z$ at low z includes too few galaxies, so these tracers can be safely used only in the range $0.4 \leq z \leq 1.0$. In contrast, the fainter luminosity-limited sample ($M_B \leq -19.3 - z$) is complete only up to $z = 0.7$, but can be used starting from $z = 0.1$. In Fig. 2 we show the comparison between the density computed with flux limited tracers and volume limited tracers.

Finally, different weights can be assigned to the tracer galaxies. For example, we can weight galaxies by their stellar mass or their luminosity in a given band, or simply by their number. As this is a subtle issue for what concern the general definition (and thus interpretation) of local density itself, we discuss explicitly advantages and drawbacks of different weighting schemes in the following section.

3. The mass-weighted density and the colour-density relation

It has been shown that galaxy formation is "biased", in the sense that galaxies have been formed earlier in higher matter-density peaks (see for example Marinoni et al. 2005). This suggests that the galaxy total mass, if not even the (dark) matter distribution on larger scales, is a key ingredient to understand galaxy formation and evolution. Moreover, we know that galaxy stellar mass correlates with the dark matter halo mass, for both early and late type galaxies (Mandelbaum et al. 2006; Yang et al. 2008). This leads to the idea that a density estimator that takes into account the stellar mass of the tracer galaxies could be more physically motivated than simple galaxy counts. From now on, we will define these two different environment parametrizations as "mass-weighted density" (MWD) and "count-weighted density" (CWD). We also refer the reader to Kovac et al. (2009), who study in detail how the reconstructed galaxy density field within the zCOSMOS 10k-sample relates to the underlying matter density field.

The concern in using the MWD is the existence of a correlation between stellar mass and other galaxy properties. The possible environmental dependence of these properties risks to be spuriously increased by their dependence on mass. A typical example, that moreover is the one we are mostly interested in, is the colour-mass relation. The left panel of Fig. 3 shows the fraction of red ($U - B \geq 1.0$) galaxies as a function of the density contrast, in equipopulated density bins, for the same luminosity-selected volume-limited sample used for the computation of the density contrast, in the redshift range $0.5 \leq z \leq 0.7$ (this cut leaves us with roughly 1200 galaxies). Density is computed with the 5th nearest neighbour method, using the fainter volume limited tracers ($M_B \leq -19.3 - z$). Orange triangles are for MWD, while red squares are for CWD. Vertical error bars are computed applying the binomial formula (see Sect. 4 for details). The dashed line is the linear fit of triangles, the solid line the linear fit of

squares. The slopes of the fits with their errors are 0.31+/−0.03 and 0.21+/−0.04 for MWD and CWD respectively. We note that the colour-density relation appears to be stronger and more significant using MWD.

We tested the influence of the underlying colour-mass relation on this slope change by shuffling galaxy properties, while preserving their coordinates and redshift. The shuffle has been performed by assigning to each galaxy the complete set of properties (mass, colour, luminosity...) of another galaxy chosen randomly in the same narrow redshift bin. We are aware that this choice can make the randomization not ideal, as galaxy properties are not completely un-correlated with galaxy 3D positions, but in this way we preserve the redshift distribution of galaxy properties. We then recalculated the CWD and MWD using the real galaxy positions, but the randomly assigned masses. This way, the CWD estimate does not change, but the 3D mass distribution (as traced by galaxy stellar mass) is not linked any more to galaxy position, and thus the MWD estimate is different from the original one.

The right panel of Fig. 3 shows the colour-density relation for the same galaxies as in the left panel, but in this case we used the new CWD and MWD and the "shuffled" colours. Symbols are the same as in the left panel. As expected, there is no significant colour-density relation when using the CWD and the random colours, as these colours are completely uncorrelated with the original galaxy position. The measured slope of the linear fit is 0.06+/−0.04. The fit is not totally flat, possibly due to the non-optimal randomization. On the contrary, when we use the MWD, we do see a colour-density relation (the measured slope of the linear fit is 0.14+/−0.03). As we know that the colour is no more (or very weakly) related to the galaxy position, but it does depend on mass, the difference that we see in the colour-density relation when using CWD and MWD is a spurious effect produced by the colour-mass relation. Although the mass-weighted density may be considered a physically motivated environment estimator, this test suggests us that it is safer to use the density computed with pure counts. Thus we will use the CWD in this work.

Summarizing our overall choice, in this work we will use a density contrast estimator based on the 5th n.n. method, computed with volume-limited and "count-weighted" tracers.

4. Redshift evolution of environmental effects

As a first step, we want to exploit the broad redshift range covered by the zCOSMOS 10k-sample to investigate the evolution with cosmic time of environmental effects on galaxy properties. If we could constrain the epoch (if any) at which environment begins playing a role in galaxy evolution, and understand whether the properties of galaxies residing in different environments evolve differently with cosmic time, we could shed more light on galaxy evolution mechanisms.

In this analysis, we want to use the density computed with the bright volume limited tracers complete up to $z = 1.0$ ($M_B \leq -20.5 - z$). As discussed in Sect. 2.4, with these tracers we can reliably measure the density only for $z \geq 0.4$. So we restrict this study to the redshift range 0.4–1.0.

The galaxy set used for this analysis is the luminosity-selected volume-limited subsample that corresponds to the bright tracers galaxies. As explained in Sect. 2.4, the dimming of 1 mag per unit redshift interval is an average evolution that should include roughly the typical passive evolution of the majority of galaxy types. The value of the intercept is chosen to have a complete sample at $z = 1$. This limit allows us to approximately follow an homogeneous and complete galaxy population up to $z = 1$. With this cut in luminosity, and considering the redshift range $0.4 \leq z \leq 1.0$, we are left with a total sample of 1133 galaxies (out of 3868 galaxies in the flux limited sample over the same redshift range).

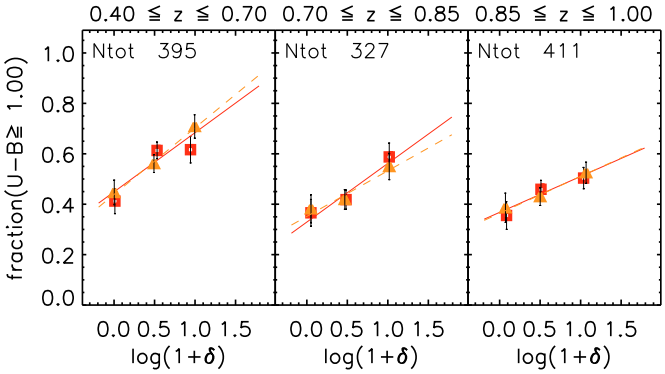

Fig. 4. Fraction of red galaxies as a function of the density contrast. Galaxies are defined "red" when they have $(U - B) \geq 1.0$. Different symbols are for different density measurement methods: red squares for bright volume limited tracers ($M_B \leq -20.5 - z$), while orange triangles for flux limited tracers. The values on the x axis represent the median density values in each density bin. The continuous red line is linear fits of the squares, and dashed orange line is the linear fit of the triangles. Their slopes with associated errors can be found in Table 1. "Ntot" is the total number of galaxies considered in each panel.

We analyzed the widely studied colour-density relation, focusing on the restframe $U - B$ colour. The zCOSMOS *bright* sample is selected in the observed I-band magnitude, that corresponds to a selection in the absolute B-band magnitude at $z \sim 0.8$. This way, our sample is not affected by any significant $U - B$ color incompleteness up the highest redshift we are interested in ($z \sim 1$).

The plot in Fig. 4 shows the fraction of red galaxies (red squares) as a function of the density contrast, in three different redshift bins. Galaxies are defined "red" when they have $(U - B) \geq 1.0$. We choose this colour threshold as it is roughly in the middle of the so called green valley of the bimodal colour distribution. We keep this value fixed at all explored redshifts, as we do not see any strong evolution of the green valley location with z. The density bins are chosen so that the total sample used in this analysis (the considered 1133 galaxies) is divided into three equipopulated bins. This way the density bins in each panel are not exactly equipopulated, but the environment thresholds are constant with redshift. This implies that we are observing, at different redshifts, comparable over-/under-densities, disregarding the average evolution of the density contrast. Vertical error bars on the red fraction values are the 1σ confidence level for the binomial statistics, computed according to the approximation given in Gehrels (1986): $\sigma^2 = f_r f_b / n$, where f_r is the fraction of "red" galaxies, f_b is the fraction of "blue" ones ($=1 - f_r$) and n is the total number of galaxies in the density bin. When the fraction for which we want to compute the 1σ confidence level is zero (/one), we fix its lower (/upper) limit to zero (/one), and its upper (/lower) 1σ level at $\sigma = 0.5/n$, as suggested by De Propris et al. (2004).

We fit the colour-density relation with a linear fit (red solid line), taking into account the vertical error bars of the points. We disregarded the estimated horizontal error on the median density value, as it is so small (on average around 0.06 dex) that the error on the linear fit is dominated by the error on the red galaxies

Table 1. Slopes and their 1σ confidence levels of the linear fits shown in Figs. 4 and 5.

z range	Volume limited tracers		Flux limited tracers	
	CWD	MWD	CWD	MWD
$U-B$				
0.40–0.7	0.23 ± 0.08	0.33 ± 0.07	0.26 ± 0.07	0.44 ± 0.06
0.7–0.85	0.23 ± 0.08	0.25 ± 0.06	0.18 ± 0.08	0.25 ± 0.06
0.85–1.0	0.14 ± 0.07	0.19 ± 0.06	0.15 ± 0.07	0.20 ± 0.06
D_n4000				
0.48–0.7	0.30 ± 0.09	0.38 ± 0.08	0.38 ± 0.08	0.48 ± 0.07
0.7–0.85	0.22 ± 0.08	0.23 ± 0.07	0.19 ± 0.08	0.28 ± 0.06
0.85–1.0	0.13 ± 0.08	0.15 ± 0.07	0.11 ± 0.07	0.16 ± 0.06
EW[OII]				
0.48–0.7	-0.20 ± 0.11	-0.27 ± 0.09	-0.28 ± 0.09	-0.35 ± 0.09
0.7–0.85	-0.07 ± 0.11	-0.05 ± 0.08	-0.06 ± 0.10	-0.13 ± 0.08
0.85–1.0	-0.06 ± 0.09	-0.11 ± 0.09	-0.06 ± 0.09	-0.10 ± 0.08

Notes. The second column lists the slopes and their 1σ confidence levels of the linear fits shown in Figs. 4 and 5, that is the slopes of the $(U-B)$-, D_n4000- and EW[OII]-density relations when density is computed with volume limited tracers ($M_B \leq -20.5 - z$) and "count-weighted" density (CWD). From the third to the fifth column the same slopes are quoted, but for density computed with different tracers (volume limited and MWD, flux limited and CWD, flux limited and MWD, respectively).

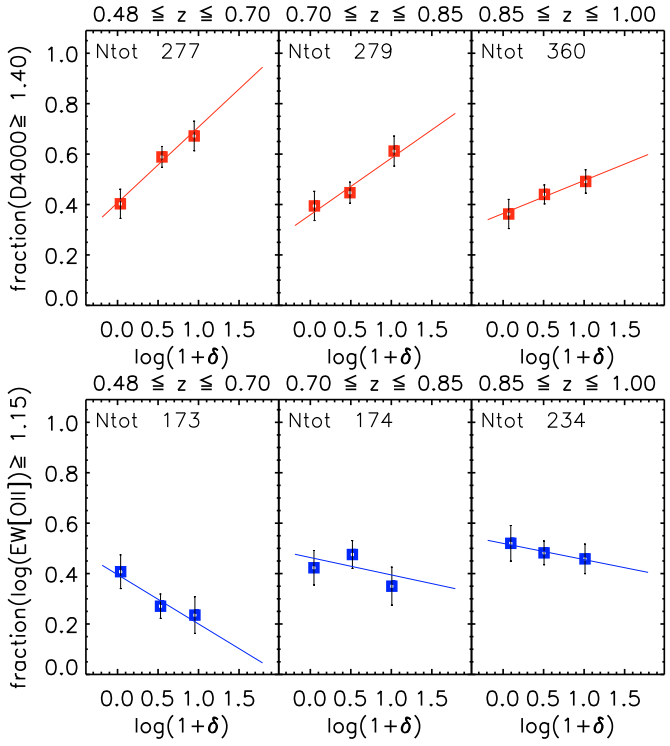

Fig. 5. *Top.* Fraction of "passive" galaxies as a function of the density contrast. Galaxies are defined "passive" when they have $D_n4000 \geq 1.40$. Symbols and lines have the same meaning as in the plots of Fig. 4. *Bottom.* Fraction of galaxies with $\log(EW[\mathrm{OII}]) \geq 1.15$ as a function of the density contrast. Symbols and lines as in the top panels.

fraction. In contrast, we verified that changing the number of density bins (compatibly with the total number of galaxies) does not change significantly the result of the fit. These considerations hold for all our subsequent analyses.

The derived slope of the linear fit and its error are quoted in the second column of Table 1. The significance associated to the colour-density trend is $\sim 3\sigma$, $\sim 3\sigma$ and 2σ from the lowest to the highest redshift bin. The colour-density relation, present at low redshift, is still present up to $z = 1$. Moreover, there is a trend of weakening of the colour-density relation for increasing redshift, as the slope of the fit becomes less steep at higher redshift.

As a reference, we list in Table 1 the slopes (and their error bars) of the linear fit of the colour-density relation that we find when using also different tracers of the local density (volume limited and MWD, flux limited and CWD, and flux limited and MWD, in the third, fourth and fifth column, respectively). The reader can notice the foreseen effect of a enhanced colour-density relation when 1) investigating the smaller scales probed by flux limited tracers and 2) using the mass-weighted density. The effect given by the flux limited tracers sample is evident at least for $0.4 \leq z \leq 0.7$, where the flux limited sample is much fainter than the volume limited one (see Fig. 1).

Usually, galaxy colours can be considered as a proxy for star formation activity, with redder galaxies having less on-going star formation. We thus analyze the dependence on environment of two other star formation indicators: the D_n4000 and the EW[OII]. In particular, D_n4000 is quite well related with the $U-B$ colour, as the U and B bands bracket the break itself. Nevertheless, the D_n4000 is a direct measure of the stellar population, and it is less affected by reddening or uncertainties due to the SED fitting necessary for the colour computation (see for example Franzetti et al. 2007).

We therefore identify two logical equivalents of our "red" galaxy sample by defining a "passive" galaxy subsample, consisting of all galaxies having $D_n4000 \geq 1.4$, and an "active" galaxy subsample including those galaxies with $\log(EW[\mathrm{OII}]) \geq 1.15$. The reader is referred to Maier et al. (2009) and Silverman et al. (2009b) for more details on the star formation activity within zCOSMOS galaxies.

These thresholds correspond roughly to the median values of the total D_n4000 and EW[OII] distributions. As for $U-B$ colour, the D_n4000 threshold does not evolve significantly with redshift, thus we used it for all the redshift bins investigated; on the contrary, the EW[OII] mean value increases with redshift, but we verified that the dependence of the "active" galaxy fraction on environment does not change significantly if we substitute the fixed threshold with an evolving one (with the exception of a different normalization).

In Fig. 5 we show the fraction of "passive" (top row) and "active" galaxies (bottom row) as a function of density, for three different redshift bins (the three columns). The symbols and the solid lines in these panels have the same meaning as those in Fig. 4. Note that these features enter the observed wavelength range at about $z = 0.48$, thus the lower limit of the first redshift bin is different from the one in Fig. 4. The slopes of the linear fits, together with their 1σ levels, are quoted in Table 1.

Figure 5 shows that the environmental effects on D_n4000 as a function of redshift mirror those on galaxy $U-B$ colour, with comparable slopes and normalizations (inside the error bars). As the "red" galaxies, the "passive" ones reside preferentially in high density regions, and this D_n4000-density relation is visible in the entire range $0.48 \leq z \leq 1$, weakening for increasing redshift. On the contrary, the fraction of "active" galaxies is higher in low densities. Even if less significant than the detection of D_n4000-density relation, we find that the EW[OII]-density relation holds up to $z \sim 1$, and like the others it becomes weaker for increasing redshift. In Table 1 we quote the slopes of the linear fits of these relations also when MWD and flux limited tracers are used to estimate the environment. As for the colour-density relation, results are compatible within errors irrespectively of the density estimator used, with a general indication for stronger

and more significant trends in the MWD case. This is mainly due to the relation between stellar mass and both D_n4000 and EW[OII], as discussed in Sect. 3. Moreover, it seems that above $z \sim 0.7$ the EW[OII] is less sensitive to environment than colour and D_n4000. A more detailed analysis of this issue is deferred to future work.

We remark that we excluded from this analysis all galaxies with low quality spectral features measurements as described in Sect. 2.2. These galaxies are ∼15% and ∼45% of the sample used for the colour-density analysis, considering the D_n4000 and the EW[OII] measurement respectively. To be sure that this spectral quality selection does not introduce any bias as a function of density, we re-computed the D_n4000- and EW[OII]- density relations considering also these previously excluded galaxies. We found results compatible (within errors) with the ones shown in Fig. 5.

Summarizing, in Figs. 4 and 5 we have shown how different galaxy properties depend on environment within a complete luminosity-selected volume-limited sample, and how these dependences evolve with redshift. Globally, these results confirm already known trends: the fraction of red galaxies is higher in high densities, and the colour-density relation becomes weaker for increasing redshift. We have also shown that the fraction of galaxies with high D_n4000 depends on environment in a way that is very similar to the $U - B$ colour (as both red colour and high D_n4000 are indicators of old and passively evolving galaxies), and this is the first time that this is shown up to $z \sim 1$. Conversely we found that the "active" galaxies (those with larger EW[OII]) reside preferentially in low densities. As for colour and D_n4000, the EW[OII]-density relation holds up to $z \sim 1$, although with less significance, and weakens for increasing redshift, further confirming the general trends observed with the other star formation indicators. We refer the reader to Sect. 8 for the comparison of these findings with previous works, and to Sect. 9 for the discussion of their implications.

The comparative study of the environmental dependences of different galaxy properties at different epochs is of crucial importance to shed more light on galaxy evolution. We defer this analysis to future work, while here from now on we will explore more in details only the colour-density relation.

5. Mass segregation as a function of environment

It has already been shown that galaxy stellar mass (M) does depend on environment, at least weakly, at both $z \sim 0.1$ and up to $z = 1.4$ (Kauffmann et al. 2004; Bundy et al. 2006; Scodeggio et al. 2009; Bolzonella et al. 2010). There is still considerable debate whether this mass-density relation is the driver of environmental effects upon other properties of a galaxy such as its colour and efficiency of star formation, given their known correlations with stellar mass. For example, in the local universe galaxy colour, D_n4000 and sSFR are found to depend on environment even when mass is fixed (Kauffmann et al. 2004; Baldry et al. 2006), but this has not been found in the range $0.2 \leq z \leq 1.4$ within VVDS data (Scodeggio et al. 2009). Although Scodeggio et al. (2009) themselves explain the possible reasons for this discrepancy, up to now no other study of this kind has been performed at intermediate-high redshift. With the zCOSMOS 10k-sample data we can now add a new insight on this issue in the range $0.1 \leq z \leq 1.0$.

The detailed analysis of the mass-density relation within the zCOSMOS data is fully described in Bolzonella et al. (2010), where the Galaxy Stellar Mass Function (GSMF) is studied for different galaxy subsamples and environments. For the sake of clarity and completeness, in this section we will simply present how we select a mass limited subsample suited for our following analysis, and how the stellar mass depends on environment in particular within this selected sample. Then, in Sect. 6 we will disentangle the triple relation among colour, stellar mass and local density.

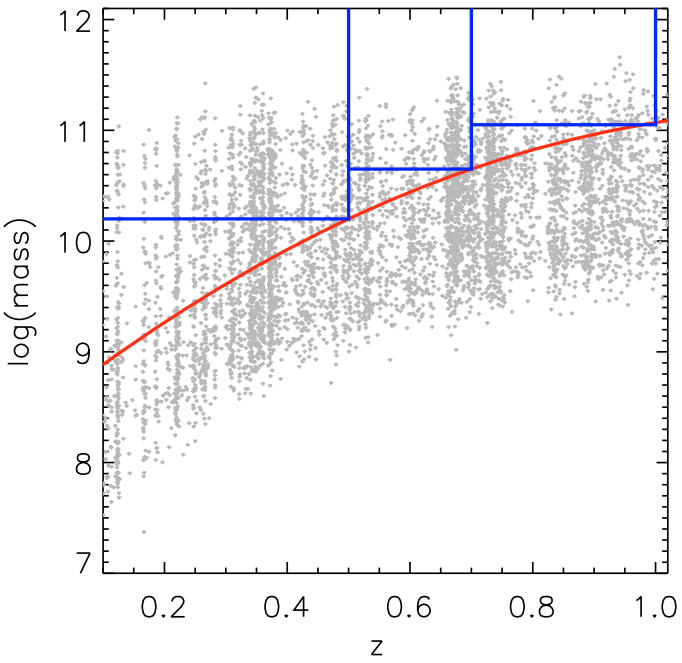

Fig. 6. The mass-redshift plane for galaxies of the 10k-sample residing in the central area of the zCOSMOS field, with red curve representing the 95% mass completeness described in Sect. 5. The three redshift bins considered in the analysis and their chosen mass limits are indicated with straight lines.

As in all flux limited samples, the range of luminosities and masses allowed in our sample varies with redshift (see Figs. 1 and 6). Given the scatter in the luminosity-mass relation, a luminosity-selected volume-limited sample at a given redshift will not be complete in stellar mass. As we now require a mass-complete sample for our analysis, we can not use the luminosity-selected volume-limited sample described in Sect. 4. Since the mass-to-light ratio (M/L) is different for different galaxy types, to select a mass-complete sample we need to identify at any redshift the smallest observable stellar mass for the red/early type galaxies, which have on the mean the higher M/L at any given mass. In practice, as proposed by Zucca et al. (2006), we fit the Spectral Energy Distribution of our galaxies to six templates (four observed spectra, Coleman et al. 1980, and two starburst SEDs, Bruzual & Charlot 1993), and we compute our mass completeness using those galaxies that have been assigned the earliest template, i.e. the E/S0 template. We define as the limit mass the mass at which we are 95% complete for these galaxies, at any given redshift. Figure 6 shows the mass-redshift plane of the 10k-sample, the red curve representing the 95% mass completeness described above.

As it can be noticed, the mass limit at $z = 1.0$ is very high. If we used it in the whole range $0.1 \leq z \leq 1.0$ in order to select a mass limited sample homogeneous at all redshifts, we would be left with too few galaxies at low z. We will also show that for the analysis carried on in this part of our work we are interested in as large a mass range as possible at any redshift. For these two reasons it is more convenient to separately adopt the smallest

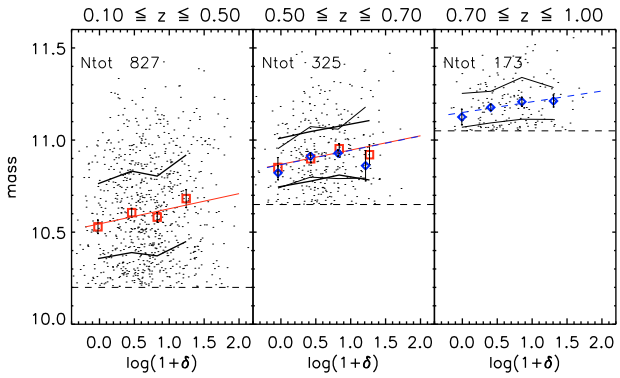

Fig. 7. Median stellar mass (red squares and blue diamonds) as a function of the "count-weighted" density contrast with volume limited tracers, for the three mass limited subsamples described in Sect. 5. Black points are single galaxies. Red squares are computed using the fainter volume limited tracers ($M_B \leq -19.3-z$), blue diamonds using the bright ones ($M_B \leq -20.5-z$). x axis values for squares and diamonds represent the median density values in each density bin. Vertical error bars associated to median stellar mass values are obtained with bootstrapping technique. Black thick(/thin) lines are the 15% and the 85% of the mass distribution in each density bin, for the faint(/bright) volume-limited tracers. Horizontal dashed lines show the mass limits in each redshift bin. The red straight lines are linear fits of the squares, the dashed blue lines of the diamonds, the slopes and their errors being quoted in the text. The total number of galaxies considered in each redshift bin is quoted in the upper part of each panel.

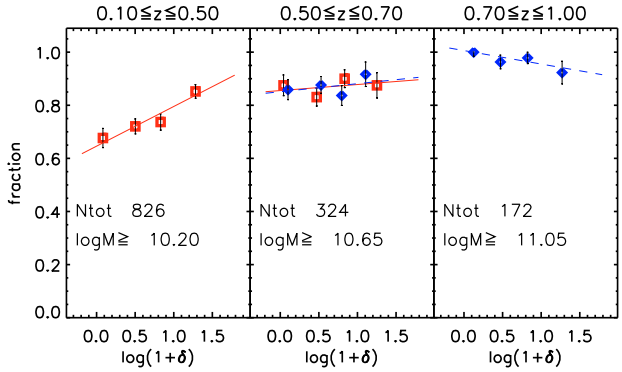

Fig. 8. Fraction of red ($U-B \geq 1.0$) galaxies as a function of density for three mass limited galaxy samples (mass lower limit in the label). Red squares are computed using the fainter volume limited tracers ($M_B \leq -19.3-z$), blue diamonds using the bright ones ($M_B \leq -20.5-z$). The values on the x axis represent the median density values in each density bin. The red straight lines are linear fits of the squares, the dashed blue lines of the diamonds, the slopes and their errors being quoted in the text. The total number of galaxies considered in each redshift bin is quoted in the lower part of each panel.

limit mass we can reach in any redshift bin. Within each z bin, we keep the limit mass constant (unlike in the case of the limiting magnitude), as it has been shown that the Galaxy Stellar Mass Function does not evolve significantly in the redshift range we are considering (e.g., Pozzetti et al. 2007).

To cover the largest available mass range we start our analysis from $z = 0.1$. This choice prevents us from using in the entire redshift range the density contrast computed with the bright volume limited tracers, as it is reliable only for $z \geq 0.4$. In contrast, the fainter volume limited tracers ($M_B \leq -19.3 - z$) represent a complete sample only up to $z = 0.7$. We decided to use the fainter volume limited tracers in the redshift interval 0.1–0.7, and the bright one for the remaining bin $0.7 \leq z \leq 1.0$. We verified that this choice does not introduce any spurious dependence on redshift, because of the change, at $z = 0.7$, of the tracers used to measure the density. We took as a reference the redshift bin $0.5 \leq z \leq 0.7$, for which we have the density computed with both the samples, and we performed all the analyses shown in Sects. 5 and 6 with both the tracers. We find that the results are always consistent using the two tracers samples, as shown for example in Figs. 7 and 8 (see the text below for the details about these figures). The same agreement is found in Bolzonella et al. (2010), where the galaxy stellar mass functions in low and high density environment are computed for both tracer types. Therefore we believe to be safe the comparison of our analysis at $z \leq 0.7$ and $z \geq 0.7$ using fainter and brighter tracers, respectively.

In summary, we selected the three redshift bins [0.1–0.5], [0.5–0.7], [0.7–1.0], with the mass limits $M_{\rm lim}$ given by $\log(M_{\rm lim}/M_\odot) = 10.2$, 10.65 and 11.05 respectively. We then studied the mass-density relation within these mass limited samples. This is shown in Fig. 7, where we plot the median stellar mass (red squares and blue diamonds) as a function of density. Red squares are computed using the fainter volume limited tracers, blue diamonds using the bright ones. The density bins are chosen in the following way. For the fainter tracers, we selected all the galaxies in the range $0.1 \leq z \leq 0.7$ with $\log(M/M_\odot) \leq 10.65$ (our highest mass limit for $z \leq 0.7$), and then we divide this sample in 4 equipopulated density bins. Then we use the so-found density thresholds in the two redshift bins 0.1–0.5 and 0.5–0.7. Similarly, for the brighter tracers we took all the galaxies with $\log(M/M_\odot) \leq 11.05$ within $0.5 \leq z \leq 1.0$, we divide this sample in 4 equipopulated density bins, and we use these density thresholds in the two redshift bins 0.5–0.7 and 0.7–1.0. The red lines in Fig. 7 are linear fits to the squares, the blue dashed lines to the diamonds. The slope values and their errors are 0.9 ± 0.03 and 0.8 ± 0.04 for the squares in the first and second redshift bin, and 0.8 ± 0.04 and 0.6 ± 0.03 for the diamonds in the second and third redshift bin, respectively.

It can be noticed that the median mass depends on environment at $z < 0.5$, but this dependence weakens for higher redshift. This may not be a pure time-evolution effect, because also the mass limit changes with redshift. Considering only the mass limited sample in $0.1 \leq z \leq 0.5$, we verified that within this sample the mass-density relation weakens when increasing the mass limit. These findings are in agreement with Bolzonella et al. (2010), who show that the GSMFs in the 10k-sample in the low and high density regions differ mainly in the low-mass part, with this difference decreasing for higher redshift.

6. Are the environmental effects on galaxy colour driven by mass?

In the previous sections we have shown how galaxy $U - B$ colour and stellar mass depend on environment. It is also well known that colour depends on stellar mass, thus we want to study whether the environmental dependence of $U-B$ is simply the effect of the combined colour-mass and mass-density relations. We address this issue studying the threefold relation among density contrast, stellar mass and colour. In the following subsections we study the colour-density relation in the mass limited samples (Sect. 6.1) and then we discuss how to disentangle the colour-mass-environment relation (Sect. 6.2).

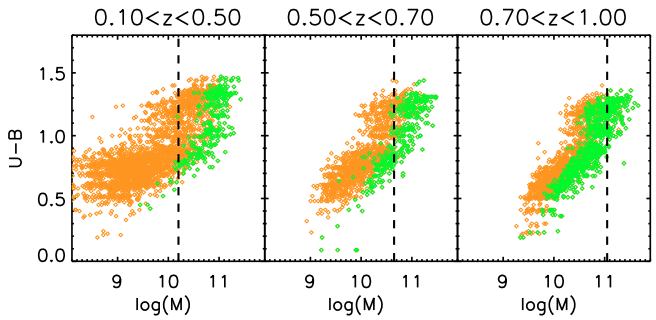

Fig. 9. The colour-mass plane for 3 different redshift bins. Orange points are all the galaxies in the redshift bin considered, green points are those galaxies that respect the luminosity limit as in Fig. 4 and vertical lines represent the mass limit at each redshift.

6.1. The colour-density relation in mass-limited subsamples

The three panels of Fig. 8 show the fraction of red ($U - B \geq 1.0$) galaxies as a function of density for the three mass limited samples presented in Sect. 5. Red squares are for fainter volume limited tracers, and blue diamonds for the brighter ones. The density bins along the x axis are selected as in Fig. 7. The linear fits to the squares and diamonds are represented with solid and dashed lines, respectively. For these fits, we find the following slopes (and 1σ confidence level): 0.17 ± 0.04 and 0.05 ± 0.05 for the squares in the first and second redshift bin, and 0.05 ± 0.06 and -0.01 ± 0.05 for the diamonds in the second and third redshift bin, respectively. We find that there is a clear colour-density relation within the mass-limited sample in the lowest redshift bin, but we do not detect it at $z > 0.5$. We remind the reader that this different behaviour at different redshift may not be a pure evolutionary effect, because in this figure we consider samples with different lower mass limits (see also the last paragraph of Sect. 5). We do not want to make any statement about galaxy evolution inspecting Fig. 8.

It can be noticed that results presented here are quite different from the ones in Fig. 4, where a luminosity-selected volume-limited sample was used and where the colour-density relation was steeper and with a lower normalization. To understand these differences we inspect Fig. 9. For the three z bins of Fig. 8, it shows the colour-mass plane for all the galaxies (orange points), with green points representing the galaxies considered in the luminosity-selected volume-limited sample of Fig. 4 ($M_B \leq -20.5 - z$) and the vertical lines the mass limits of Fig. 8.

The higher normalization in Fig. 8 is explained by the fact that with the chosen mass limits we select an higher fraction of red galaxies. This effect increases with z, up to the highest redshift bin, where almost only red galaxies are selected. This observation suggests that the fixed colour cut at $U - B = 1$ to define red galaxies is not well suited for the study of our mass-selected samples, and we will expand on this point in the next subsection.

We also notice how the colour-density relation for the mass-selected sample within $0.5 \leq z \leq 0.7$ (middle panel in Fig. 8) is significantly flatter than the one obtained for the luminosity-selected volume-limited sample within roughly the same redshift interval ($0.4 \leq z \leq 0.7$, first panel of Fig. 4). Observing the second panel in Fig. 9, we see that the explanation for this flattening is related to the different galaxy populations that are selected using luminosity or mass limits. In the luminosity-selected volume-limited sample there is a population of lower-mass blue galaxies that is not present in the mass limited sample due to their low M/L. Moreover, this population has no red counterpart (at the same mass) in the luminosity selected sample, as these redder galaxies are too faint to satisfy the luminosity-selection criterion (they have on the mean an higher M/L).

This tail of less massive blue galaxies that we find in the luminosity-selected sample inhabits preferentially low density regions. This can be deduced noticing that the red fractions in Fig. 4 are on average always lower than those in Fig. 8, but the percentage difference is much larger in the low density bins. It remains to be clarified whether these galaxies reside mainly in low density environment only because of their low mass (the mass segregation effect that we showed in Fig. 7 and that is detailed in Bolzonella et al. 2010), or because environment also plays a role in shaping their colour. We will disentangle this dependence in the following subsection.

Here, it is worth remarking the following. We are aware that the M/L spread is particularly large in our sample because of the relatively blue band-passes we use (U- and B-band). These bands are more sensitive to dust reddening, and moreover the light at these wavelengths is dominated by younger stars, that not only are a small fraction of the mass, but also can be the product of transient phenomena, such as sudden bursts of star formation. As already explained, our choice of the B-band for the luminosity selection and of the $U - B$ colour for the analysis is dictated by the fact that the I-band flux limit of our survey ($I_{AB} \leq 22.5$) corresponds at the rest frame B-band at $z \sim 0.8$. This allows our sample to be not significantly affected by colour incompleteness in the redshift range we are interested in ($z \lesssim 1$). Moreover, in a luminosity-selected sample the M/L spread is in general unavoidable, irrespectively of the band used for the selection, because it is produced at least by the variety of star formation histories. This gives rise in turn to a large spread in stellar masses, and together with the colour-mass relation, this causes the colour-density relation in a luminosity-selected sample to be strongly biased by the mass-density relation. In a mass-limited sample this bias is weaker, as the allowed mass range is smaller, but the mass-density relation does not disappear. Thus, if we want to study the direct environmental effects on galaxy properties, such as the colour, without being biased by the mass segregation as a function of environment, we need to select our sample(s) in narrow mass bins.

6.2. Disentangling the colour-mass-density relation

Following the discussion detailed above, in this section we study the colour-density relation in mass bins, in order to understand whether it is only the result of combining the mass-density and colour-mass relations. First, we divide the three mass limited samples in mass bins of $\Delta \log(M/M_\odot) = 0.2$, in order to cancel the mass-density relation. We verified that in such narrow mass bins the stellar mass does not depend any more on environment. Secondly, as previously discussed, the colour cut at $U - B = 1$ is not well suited to define "red" galaxies in a sample with $\log(M/M_\odot) \gtrsim 10.7$, thus we introduce a new definition of "red" galaxies. We take a colour threshold roughly parallel to the red sequence in the colour-mass plane, and ~0.3 mag bluer than the red sequence itself. We used as reference the red sequence in the first redshift bin of Fig. 9. This colour threshold depends on the stellar mass, as the red sequence becomes redder for higher masses. The first panel of Fig. 11 shows the colour-mass plane within $0.1 \leq z \leq 0.5$. The red line is the chosen colour threshold. As it is always redder than $U - B = 1$, we define as "very red galaxies" those galaxies with a colour redder than this threshold.

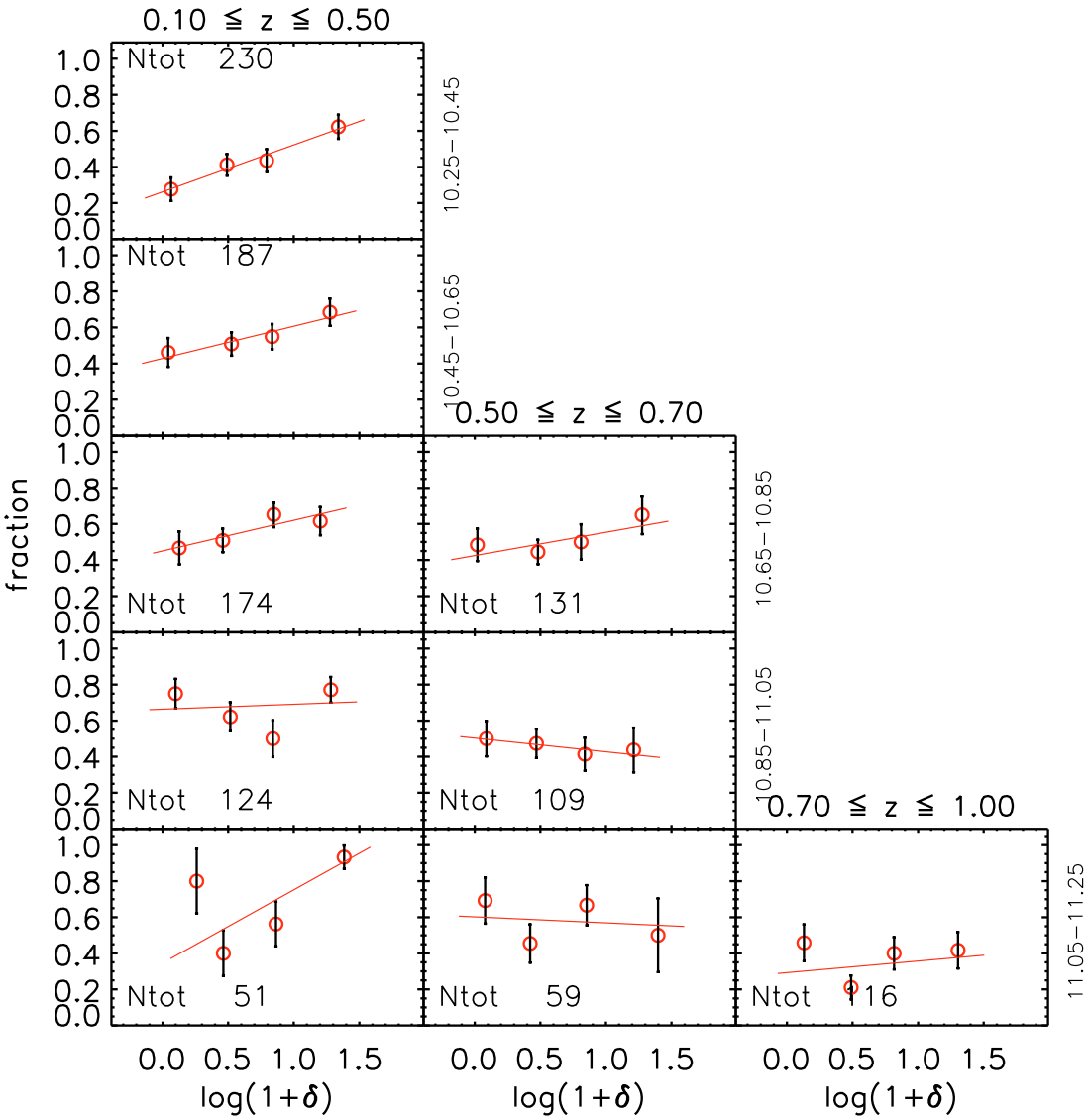

Fig. 10. Colour-density relation using number density and volume limited tracers for subsamples of galaxies divided in three redshift bins (columns, redshift bins quoted on *the top*) and five mass bins (rows, mass bins quoted *on the right*, in logarithmic scale). For $z \leq 0.7$ we use the fainter volume limited tracers ($M_B \leq -19.3 - z$), for $z \geq 0.7$ brighter ones ($M_B \leq -20.5 - z$). Red circles show the fraction of galaxies with $U - B$ colour redder than a threshold that depends on the stellar mass, as shown by the diagonal red line in the first panel of Fig. 11 (see also text for details). The values on the x axis are the median density values in each density bin. Red lines represent the linear fit of circles. Their slopes and associated 1σ confidence levels are quoted in Table 2. In each panel, "Ntot" is the total number of galaxies in that mass and redshift bin, while the number of galaxies satisfying the colour threshold is quoted in Table 2.

In Fig. 10 we plot the fraction of "very red" galaxies (red circles) as a function of the density contrast. The columns are for three redshift bins as indicated on top (the same as in Fig. 8), while the rows represent different mass bins: from top to bottom we consider the bins 10.25−10.45, 10.45−10.65, 10.65−10.85, 10.85−11.05 and 11.05−11.25 in $\log(M/M_\odot)$ units, as indicated in the labels on the right of the right-most panels. The lowest mass considered in each redshift bin is always equal or bigger than the mass limit at that given z. For this analysis we used CWD and fainter volume limited tracers for $z \leq 0.7$, and CWD and brighter volume limited tracers for $z \geq 0.7$. We verified that our results in the range $0.5 \leq z \leq 0.7$ do not change using fainter or brighter volume limited tracers. The dashed-dotted line is the linear fit of the circles (considering their error), and "Ntot" indicates the total number of galaxies in each panel. Table 2 shows the fit slopes with their error, together with the number of "very red" galaxies.

Figure 10 shows that the fraction of "very red" galaxies seems generally not to depend on environment once mass is fixed, but we can notice some exceptions. In fact, in the redshift range $0.1 \leq z \leq 0.5$ we see that the fraction of "very red" galaxies depends on environment for $\log(M) \lesssim 10.7$. This fraction seems to show some trend with density also for the highest masses explored ($\log(M/M_\odot) \gtrsim 11.0$), but for these high masses we have larger error bars due to the lower statistics. We note that the same trend is observed by Tasca et al. (2009), when they study the fraction of the more massive early type galaxies as a function of local density. We will explore this mass regime with higher statistics with the complete zCOSMOS bright sample.

We addressed this issue more in detail, focusing our attention on the redshift range $0.1 \leq z \leq 0.5$, where the colour-mass-density relation can be better studied thanks to the larger mass range spanned above the mass limit. The aim is to analyze in a

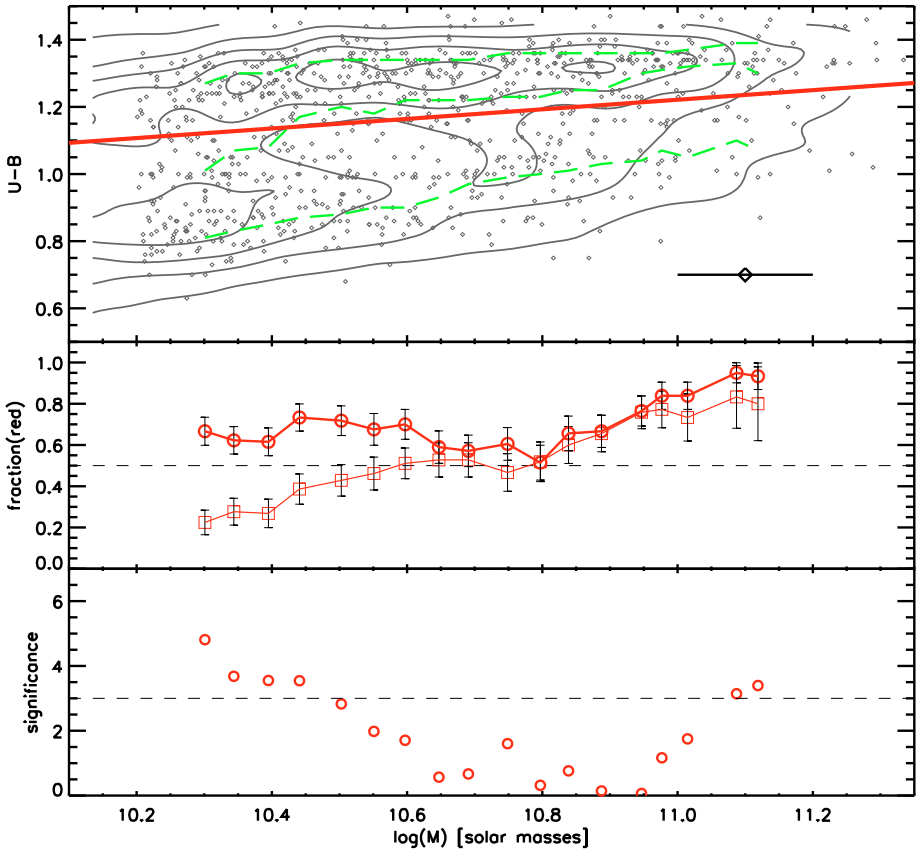

Fig. 11. *Upper panel*: colour-mass plane for galaxies in the redshift range $0.1 < z < 0.5$, above the mass limit $\log(M/M_\odot) = 10.2$. Green dashed lines represent 15%, 50% and 85% of the color distribution, in bins of 0.2 in mass (logarithmic scale, as represented by the horizontal line in the bottom right corner). Black contours are the isodensity contours of the plotted points. The red straight line is the colour thresholds used to define "very red" galaxies. It is a straight cut following roughly the red sequence and 0.3 magnitudes bluer than the red sequence itself. *Middle panel*: in not-independent bins of 0.2 in $\log(M/M_\odot)$ units, thick circles are the fraction of "very red" galaxies in the highest density quartile and thin squares in the lowest density quartile. The horizontal dashed line at fraction = 0.5 is for reference. *Bottom panel*: the significance of the slope of the linear fit of the red fraction as a function of density, in each mass bin. In these panels, density is computed with fainter volume limited tracers and without mass weights.

Table 2. Slopes of the linear fits plotted in the panels of Fig. 10.

Mass range	$0.1 \le z \le 0.5$		$0.5 \le z \le 0.7$		$0.7 \le z \le 1.0$	
	Slope $\pm 1\sigma$	N_{vr}/N_{tot}	Slope $\pm 1\sigma$	N_{vr}/N_{tot}	Slope $\pm 1\sigma$	N_{vr}/N_{tot}
10.25–10.45	0.26 ± 0.07	101/230	–	–	–	–
10.45–10.65	0.18 ± 0.07	101/187	–	–	–	–
10.65–10.85	0.17 ± 0.10	99/174	0.13 ± 0.10	65/131	–	–
10.85–11.05	0.03 ± 0.08	83/124	-0.08 ± 0.12	50/109	–	–
11.05–11.25	0.41 ± 0.12	33/51	-0.03 ± 0.16	33/59	0.06 ± 0.11	42/116

Notes. Different rows are for the different mass ranges, and the columns for the three redshift bins. N_{vr} is the number of "very red" galaxies, and N_{tot} the total number of galaxies in each panel.

more continuous and smooth way the colour-density relation as a function of mass bins.

The first panel of Fig. 11 shows a zoom-in of the first panel of Fig. 9, but in this case only above the completeness mass limit $\log(M/M_\odot) = 10.2$. The black solid curves are the density contours and the green dashed lines are the 15th, 50th and 85th percentiles of the colour distribution in not-independent mass bin of $\Delta \log(M/M_\odot) = 0.2$, each shifted from the previous one by $\Delta_{shift} \log(M/M_\odot) = 0.05$. In this panel we show with a red diagonal line the colour threshold used also in Fig. 10 to define "very red" galaxies. For each mass bin, we computed the fraction of "very red" galaxies in four density bins, defined as in Fig. 10. In the second panel of Fig. 11 we plotted the very red galaxy fraction for the lowest and highest density bins, with squares and circles respectively. Then in each mass bin we computed a linear fit of the four fraction values as a function of density, and in the third panel of Fig. 11 we plotted the significance (the σ level) of the slope of these fits. The horizontal dashed line is the 3σ significance level, for reference.

Figure 11 more clearly shows the results of Fig. 10. If we fix the galaxy stellar mass, some colour-density relation is still measurable at least at a 3σ significance level for galaxies with

$\log(M/M_{\odot}) \lesssim 10.6$. We note that for these low masses the galaxy population is still composed by two main colour sequences, or clouds, divided by the so called green valley. On the contrary, according to the colour-mass relation, galaxies with higher masses have mainly redder colours.

The central panel of Fig. 11 indirectly shows also that a colour-mass relation holds irrespectively of environment. In fact the definition of "very red" galaxies implies that we select redder and redder galaxies for higher masses. We see that the fraction of "very red" galaxies in high densities is almost constant as a function of mass and this means that in this environment galaxy colour becomes globally redder with increasing mass. The reddening of the galaxy population for higher masses is even more evident in low density regions, where the fraction of "very red" galaxies increases as a function of stellar mass.

Finally, we observe that the fraction of "very red" galaxies seems to have some (weaker) dependence on the density contrast also for the highest masses explored. Unfortunately the number of such massive objects in our sample is quite low (less than 100 galaxies in each of the last three mass bins of Fig. 11), and so the observed relation between density and the "very red" galaxy fraction is not significant (if real). It will deserve a deeper investigation, once the complete zCOSMOS *bright* sample will be available (almost doubling the statistics of the 10k-sample).

7. Scale dependence of environmental effects

In the previous sections we have studied environment on the shortest scales on which we could compute it, given the limits imposed by the mean interparticle separation of the galaxies in our sample, and thus the limits of density reconstruction reliability found using mock catalogues (Kovač et al. 2010a). Moreover, we used volume limited tracers for the reasons listed in Sect. 2.4, while flux limited tracers can probe shorter scales (see Fig. 13 in Kovač et al. 2010a).

The issue of the scale on which density is computed is yet of great interest. For example, a still open question is whether the effects seen on large scales are only "residual" of those seen at smaller scales, or whether they add information. Some works at $z \sim 0.1$ carried out with SDSS and 2dFGRS data (Kauffmann et al. 2004; Blanton et al. 2006) assess that environmental dependence of galaxy properties on scales larger than 1 h^{-1} Mpc are driven only by the influence of scales ≤ 1 h^{-1} Mpc. It could be interesting to extend this study at higher redshift, to provide clues for any interpretation of their results, and also possibly to add useful information for planning future survey strategies.

We thus tried to address this issue using our available data. While Kauffmann et al. (2004) and Blanton et al. (2006) used cylindrical filters with fixed radii, within zCOSMOS 10k-sample we can not reach scales as small as ~ 1 h^{-1} Mpc with a fixed aperture, as explained in Sect. 2.3. This is expected due to the high mean interparticle separation of the 10k-sample, that increases from ~ 3 h^{-1} Mpc to ~ 7.5 h^{-1} Mpc in the range $0.1 \leq z \leq 1.0$. We do reach scales smaller than 1 h^{-1} Mpc only with the 5th n.n. technique, using flux limited tracers, and only when considering very high densities.

To be more precise, as one can see in Fig. 13 in Kovač et al. (2010a), using flux limited tracers and the 5th n.n. method we reach scales below 1 h^{-1} Mpc for overdensities ($\log(1+\delta) \geq 0$) only within $z \lesssim 0.5$.

Of course using an adaptive scaling (5th n.n.) as a reference is not trivial, as scale varies with density. Nevertheless, we addressed this issue following an approach similar to the one shown in Fig. 14 of Kauffmann et al. (2004). This figure shows that the median value of D_n4000 depends on the number of galaxy neighbours, on both small (1 h^{-1} Mpc) and large (5 h^{-1} Mpc) scale. The question is whether the density on the larger scale still has effects on galaxy D_n4000 once the density on the smaller scale is fixed. Kauffmann et al. (2004) show that median D_n4000 does not depend on large scale environment, once the small scale density is chosen to be enclosed in a small range of very low densities or very high densities. We reproduce this analysis within the zCOSMOS 10k-sample. We consider the density computed on a 5 h^{-1} Mpc Gaussian filter as the large scale environment, and we use the 5 th n.n. as the density on the smaller scale, of course paying attention at the variation of this scale itself with density. We will call these densities [5g] and [5th] respectively. Our result is shown in Fig. 12. The figure is divided in 4 panels.

The top left panel shows the fraction of red galaxies ($U-B \geq 1.0$) for the subsample of galaxies within $0.1 < z < 0.5$ and with $M_B \leq -18.5 - z$, as a function of the density contrast. The density is computed with flux limited tracers, and without mass-weights, for both the [5th] (red diamonds) and the [5g] (blue triangles). The value of the slope of the colour-density relation is compatible within the two density estimators (scales), but with the [5th] we reach higher densities, where we observe the highest red fraction.

The top right panel shows the relation between [5th] and [5g] densities, on the x and y axis respectively. The solid line represents the bisector, for reference. It can be noticed that for the lowest densities, the two environment estimators are very similar. This is due to the fact that the distances from the 5th n.n. are getting closer to the scale of the [5g]. On the contrary, for high densities, the [5th] density contrast reaches values well above the maximum spanned by [5g], because of the smaller and smaller scales probed by the [5th].

In the bottom panels we want to test whether some environment-colour relation is still present on larger scales ([5g]), when selecting narrow bins of densities on small scales ([5th]), and vice-versa.

The bottom-left panel of Fig. 12 shows the following. We divided the [5th] density distribution in equipopulated bins of roughly 300 galaxies (x axis), and for each of these bins we plot the fraction of red galaxies in the first and last quartile of the [5g] density distribution (thick symbols are for the highest density bin, light symbols for the lowest density bin). No trend with density on large scale is left, if we fix the small scale density.

The bottom-right panel shows the opposite analysis. For any equipopulated bin of [5g] density (x axis), we plot the fraction of red galaxies in the first and last quartile of the [5th] density distribution in that bin. In this case, we see that a quite strong trend with density on small scale is left, if we fix the large scale density. This is more evident where [5th] reaches smaller scales, that is for higher densities.

From these plots, we conclude that galaxy $U-B$ colour is affected by small scale (<1 h^{-1} Mpc) environment, while it apparently depends on the local density on larger scale only as a mirror of the dependence on small scale. This at least it is true up to $z = 0.5$, and for a sample of galaxies with $M_B \leq -18.5 - z$. Unfortunately it is not possible with our data to extend this study above this redshift, as we do not reach scales small enough (<1 h^{-1} Mpc) given the increase of the mean interparticle separation.

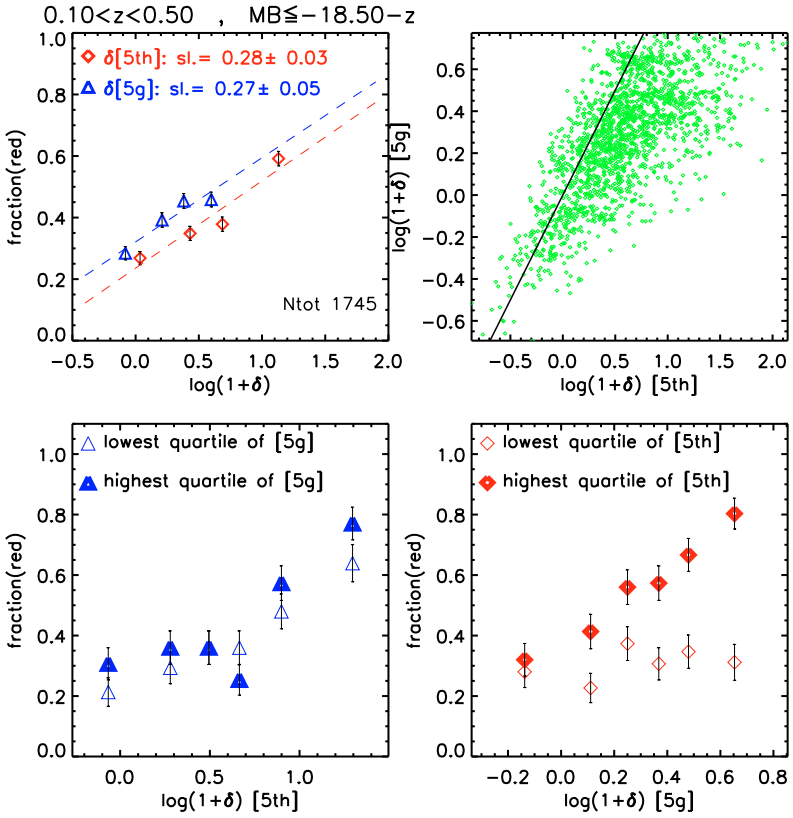

Fig. 12. *Top-left panel*. Colour-density relation for galaxies with $M_B \leq -18.5 - z$ and $0.1 < z < 0.5$. We use CWD computed with flux limited tracers. Red diamonds are for the 5th n.n. density estimator ([5th]), while the blue triangles for the density computed with a 5 Mpc Gaussian filter ([5g]). x axis values are the median value in four roughly equipopulated bins of the density distribution, vertical error bars are given by the usual binomial formula. "Ntot" is the number of galaxies in the subsample, while the linear fit slope value is quoted with its error for both the densities. *Top-right panel*. Scatter plot of [5th] (x axis) and [5g] (y axis) densities. The straight line is the bisector. *Bottom-left panel*. For any small bin of [5th] density (x axis, equipopulated bins of 300 galaxies), we plot the fraction of red galaxies in the first and last quartile of the [5g] density distribution (thick symbols are for the highest density bin, light symbols for the lowest density bin). *Bottom-right panel*. The opposite of the bottom-left panel. For any small bin of [5g] density (x axis), we plot the fraction of red galaxies in the first and last quartile of the [5th] density distribution (same symbols as in the bottom-left panel).

8. Comparison with other works

Environmental effects on galaxy properties have already been studied within other data sets up to $z \sim 1$ and above. Considering in particular spectroscopic surveys, the colour-density relation has been analyzed within the VIMOS-VLT Deep Survey (VVDS) and the DEEP2 Galaxy Redshift Survey. Our results are qualitatively in agreement with their findings, showing that the colour-density relation in a luminosity selected sample weakens for increasing redshift.

More in detail, using VVDS data (a purely flux limited galaxy sample with $I_{AB} \leq 24.0$) Cucciati et al. (2006) show that galaxy colour depends on the density contrast, with increasing strength for lower redshifts and for brighter galaxies. They show also the absence of the colour-density relation at $z \sim 1$, and a possible reversal of the relation itself for $z > 1.2$, for luminosities around $M_{B(H_0=70)} \leq -21.27$. In the luminosity and redshift ranges that we have in common, we find that our results (Fig. 4) are consistent with those presented in Cucciati et al. (2006), even if we are using here a slightly different density estimator. Our results of Fig. 4 are in agreement also with the ones obtained with DEEP2 data, as shown by Cooper et al. (2007) when they use a purely luminosity selected sample (although their definition of red galaxy does depend on absolute magnitude).

We remark that Cooper et al. (2007) obtain quite different results if they use a second differently selected sample. They show that the colour-density relation is still present at $z \sim 1$ and disappears only at $z \sim 1.3$ if they use a luminosity-selected sample with a colour-dependent luminosity limit, the limit being brighter for redder galaxies. In Sect. 6.1 we discussed the risk of analyzing the colour-density relation in a luminosity selected sample, and the colour-dependent luminosity limit used by Cooper et al. (2007) may further decrease the control on biasing effects. The selection that they use includes only bluer galaxies at faint luminosities, while redder galaxies are included if they are bright. This means that the underlying spread in mass versus luminosity becomes luminosity (or colour) dependent, producing a non trivial effect caused by the mass-density relation.

Our results on the EW[OII]-density relation (Fig. 5, bottom panels) are also in agreement with those obtained with the DEEP2 data (Cooper et al. 2006), although we find a less significant EW[OII]-density relation within $0.85 \leq z \leq 1$.

Our findings are qualitatively in agreement also with those found by Scoville et al. (2007a), based on the entire COSMOS data set, with the density field computed using photometric redshifts. In particular, they find that more massive objects reside preferentially in higher densities, where also the fraction of "Early Type" galaxies is higher, and this is true at all redshifts

explored ($0.2 \leq z \leq 1.1$). Moreover, they find that the median value of τ_{SF}, defined as the inverse of the specific star formation rate (sSFR), is higher in more dense environment, and this dependence weakens for higher redshifts. This is in agreement with our results on EW[OII], that is a proxy for the sSFR (thus $\sim 1/\tau_{SF}$).

Finally, it is interesting to compare our results about the colour-density relation at fixed mass with similar works. In the local universe, Baldry et al. (2006) find that the fraction of galaxies in the red sequence is higher in more dense environments at any given mass in the range $9 \leq \log(M/M_{\odot}) \leq 11$. Kauffmann et al. (2004) show similar results considering the dependence of D4000 Å break and specific star formation rate on local density at fixed stellar mass. More in details, Baldry et al. (2006) find that the difference between the fraction of red sequence galaxies in the lowest and highest densities decreases continuously for higher masses, as we also show in Fig. 11. We note that their definition of "red sequence galaxies" implies a colour threshold that becomes redder for brighter luminosities, i.e. similar to the colour threshold we adopt, that becomes redder for higher masses.

Considering higher redshift studies, we compared our results on the colour-mass-density relation to the ones presented in Scodeggio et al. (2009), based on VVDS data. While they find a mass-density relation for mass limited samples, they do not find any residual colour-density relation once fixing the stellar mass. In the redshift range that we have in common whit them ($0.2 \leq z \leq 0.7$) we can explore only stellar masses higher than the ones they study. Nevertheless, as we find a colour-density relation at fixed mass for $10.2 \lesssim \log(M/M_{\odot}) \lesssim 10.7$ within $0.1 \leq z \leq 0.5$, while they do not find it for slightly lower stellar masses in the same redshift range, we studied in detail the differences between the two analyses.

First, we observe that their red sequence in the colour-mass plane is much less populated then ours, with respect to the blue cloud. We verified this inspecting directly VVDS data, while for reference we refer the reader to Fig. 1 in Franzetti et al. (2007), where a colour-magnitude diagram is shown, mirroring the colour-mass plane. De-populating randomly our red sequence in order to lower our global fraction of red galaxies down to the value found in the VVDS sample, we find that the fraction of the remaining red galaxies is less dependent on environment than before. Secondly, Scodeggio et al. (2009) use a density contrast smoothed on a larger scale with respect to the one we use. Recomputing our colour-density relation in mass bins using the same scale they use, we obtain a weaker colour-density relation. We conclude that the differences between Scodeggio et al. (2009) and our work can be fairly explained, and that our results are robust against these differences.

9. Discussion

9.1. The evolution of the colour-density relation in a luminosity-selected sample

It is nowadays well assessed that in the local universe clear connections exist between the local environment and several galaxy properties. On average, while redder and brighter galaxies live preferentially in regions where the local density is higher, the opposite is true for bluer and fainter galaxies (e.g., Balogh et al. 2004; Kauffmann et al. 2004; Blanton et al. 2005; Hogg et al. 2004). This picture is enriched by measurements of the two-point galaxy correlation function for different luminosity and colour sub-populations. More luminous galaxies tend to be more clustered that fainter ones, and red galaxies exhibit a stronger and steeper real-space correlation function than blue galaxies (Norberg et al. 2002; Zehavi et al. 2002; Madgwick et al. 2003). Moreover, studying the luminosity function for early/red galaxies in different environments, a brighter M^* has been found for early-type galaxies residing in higher density regions, when density is computed on several Mpc scales (Croton et al. 2005); note, however, that it is not yet clear whether the early-type LF computed in clusters has a brighter M^* when compared with the LF in the field (see for example the discussion in Boselli & Gavazzi 2006).

This composite picture at low redshift is globally still valid at higher redshift ($z \lesssim 1$). On the one hand, it has been found that the colour-density relation persists at higher redshifts (Cucciati et al. 2006; Cooper et al. 2007). On the other hand, studies of galaxy clustering by luminosity, by spectral type and by stellar mass at high redshift (e.g., Coil et al. 2004a,b; Pollo et al. 2006; Meneux et al. 2006, 2008, but see also Meneux et al. 2009) have shown that red, early type galaxies at $z \sim 1$ are more strongly clustered than their blue counterparts (this is also true at all redshifts up to $z \sim 1.2$). Furthermore, the clustering length increases for more massive galaxies and for brighter ones. This is mirrored by the LF per environment studied in Ilbert et al. (2006), where it is shown that at $z \sim 1$ the brighter galaxies are preferentially populating high-density regions, while the opposite is seen for fainter galaxies.

Although it is commonly observed that the pictures at $z \sim 0.1$ and at $z \sim 1$ are linked by the progressive weakening of the environmental effects for increasing redshift (Cucciati et al. 2006; Cooper et al. 2007), it is not still totally clear when this environmental dependence was established. It has even been observed the presence at $z \gtrsim 1$ of colour-density and SFR-density relations that are the opposite with respect to the ones in the local universe (Cucciati et al. 2006; Elbaz et al. 2007; Cooper et al. 2008). Moreover, more light has still to be shed on the origin itself of these environmental effects, to understand if galaxy properties are related only to the environment in which galaxies have been born ("nature" hypothesis), or if the environment surrounding galaxies at each epoch of their evolution continuously plays a role in shaping their properties ("nurture" hypothesis).

Unfortunately, the evolution of the environmental effects on galaxy properties up to $z \sim 1$ and above has always been studied in luminosity selected samples. We have shown in the previous sections that this selection may give rise to a misleading interpretation, given the underlying mass-density relation. For example, the faster decreasing with redshift of the red fraction in high densities than in low densities, found in both Cucciati et al. (2006) and Cooper et al. (2007), at a first level can be interpreted as the proof that "nurture" is at work, differently shaping galaxy properties in different environments. But when we take into account the mass-density relation, these findings become easily interpretable with a biased galaxy formation: i) more massive galaxies formed first in the highest density peaks (e.g. Marinoni et al. 2005), and being more massive they consumed their gas reservoir more quickly, causing the fast increase of the red fraction with cosmic time in high densities; ii) low mass galaxies formed later in lower density regions, and we know that they consume their gas more slowly than their higher mass counterparts, and this is observable in the slow (or even absent) changing with time of the red fraction in low densities.

Our results are qualitatively in agreement with the above-mentioned picture, when analysis is performed within luminosity-selected samples. In Sect. 4, for a luminosity-selected volume-limited sample complete up to $z = 1$, we find

that the colour-density relation weakens for increasing redshift (Fig. 4), this trend being supported by the D_n4000-density and EW[OII]-density relations (Fig. 5), that are clearly stronger in the lowest redshift bin explored ($0.48 \leq z \leq 0.7$) than in the highest one ($0.85 \leq z \leq 1.0$)

More in details, we also find that the fraction of red galaxies (but also of both "passive" and "active", as defined for Fig. 5) in the highest density bin has a stronger variation with redshift than the corresponding fraction in the lowest density bin. The above mentioned discussion about the galaxy biased formation and the mass-density relation is well suited to explain our findings. Nevertheless, it may be the case that the faster gas consumption in high densities is not only caused by the higher masses, but it may be accelerated by physical processes taking place in high density regions. It is not possible, within our results, to distinguish which are the physical processes really at work in the overdense regions among the ones currently proposed (e.g. ram pressure stripping of gas, Gunn & Gott 1972; galaxy-galaxy merging, Toomre & Toomre 1972; strangulation, Larson et al. 1980, harassment, Moore et al. 1996, and so on). This prevents us from a more detailed analysis about the possible presence of nurture effects.

Finally, we note that the redshift evolution that we find for the colour-density relation in a luminosity-selected sample is consistent with other parallel analyses performed within the 10k-sample. Iovino et al. (2010) show that the fraction of blue galaxies $F_{\rm blue}$ in galaxy groups is lower than $F_{\rm blue}$ among isolated galaxies at any redshift in the range $0.2 \leq z \leq 1.0$, with this difference decreasing for higher redshift. Moreover, the fraction of morphologically early type is always higher in higher densities, with environment parametrized using both the density field (Tasca et al. 2009) and galaxy groups (Kovač et al. 2010b).

9.2. The role of stellar mass in the colour-density relation

Several studies indicate that, among other properties such as luminosity and morphological parameters, colour (Blanton et al. 2005) and specific star formation rate (Kauffmann et al. 2004) are the properties most tightly related to environment. In the past years it has been also shown that the galaxy stellar mass drives the star formation history of galaxies (e.g. Gavazzi & Scodeggio 1996; Scodeggio et al. 2002), that in turn is mainly responsible for the galaxy colour. Moreover, the stellar mass is related on the one side to the galaxy halo mass (Mandelbaum et al. 2006), and on the other side to the local environment as determined by nearby galaxies (Kauffmann et al. 2004; Bundy et al. 2006; Scodeggio et al. 2009; Bolzonella et al. 2010).

In particular, we refer the reader to Bolzonella et al. (2010) for a detailed study of the environmental effects on galaxy stellar mass within the zCOSMOS 10k-sample. They show that the Galaxy Stellar mass Functions (GSMF) is dominated by more massive galaxies in high densities, and that this difference between the GSMF in lower and high density environments decreases for higher redshift. We remark that these findings are mirrored by those related to the Luminosity Function (LF), based on the same data Zucca et al. (2009).

It follows that a non-biased analysis of environmental effects on galaxy colour (or on other properties) can be addressed only within complete mass-selected subsamples that span a narrow mass range.

In our work, we disentangled the three-fold dependence among galaxy colour, mass and environment. Globally, we do not find any colour-density relation up to $z \sim 1$ when mass is fixed (Fig. 10), with the exception of $\log(M/M_\odot) \lesssim 10.7$, where we see a clear colour-density relation (see also Fig. 11). As discussed in Sect. 8, this is in broad agreement with similar studies in the local universe (Kauffmann et al. 2004; Baldry et al. 2006).

Our findings about the colour-density relation at fixed mass are coherent with the general picture depicted by other parallel analyses based on the zCOSMOS 10k-sample. Tasca et al. (2009) and Kovač et al. (2010b) find the same result studying the fraction of morphologically early type galaxies as a function of the density contrast and galaxy group membership, respectively. The same hold for the study of the fraction of blue galaxies in groups and in isolation (Iovino et al. 2010).

From these results, it seems that in the redshift range $0.1 \leq z \leq 0.5$ there exists a sort of threshold mass ($\log(M/M_\odot) \sim 10.7$), below which the mix of the two broad galaxy populations (red and blue, early and late) does still depend on local density once stellar mass is fixed. Thus for low masses environment affects directly galaxy properties like at least colour and morphology.

Accordingly to these results, we asses that the colour depends primarily on mass, but for the low-mass regime the local environment modulates this dependence.

First, we show that a colour-mass relation holds irrespectively of environment. Our definition of "very red" galaxies implies a selection of redder galaxies for increasing mass. The fact that the fraction of "very red" galaxies in high densities is almost constant as a function of mass (thick circles in the middle panel of Fig. 11) means that in this environment galaxy colour becomes globally redder for higher masses. This effect is even stronger in low density regions, where the "very red" galaxy fraction increases for increasing mass. The same is shown in Bolzonella et al. 2010, studying the GSMF per galaxy types in different environments. In parallel, this behaviour is also observed in the Luminosity Function (Zucca et al. 2009).

Second, in this scenario where a colour-mass relation is embedded in both low and high density regions, the environment seems to have a role in shaping different colour distributions in the redshift range $0.1 \leq z \leq 0.5$ once mass is fixed. This means that environment does play a role independently of stellar mass. For example, in the central panel of Fig. 11 we see that the fraction of red galaxies is clearly a function of the density contrast at any given mass below $\log(M/M_\odot) \sim 10.7$ (the possible presence of a similar trend for $\log(M/M_\odot) \sim 11.1$ is discussed in Sect. 6.2). Continuing the comparison with the parallel analysis on the GSMF, also in Bolzonella et al. (2010) the role of environment on galaxy colour per mass bin emerges clearly. The fractional contribution of the separated blue and red galaxies GSMFs to the global GSMF varies with environment, especially in the range of intermediate masses ($9.5 \lesssim \log(M/M_\odot) \lesssim 10.5$).

A possible general picture to describe these findings is the following. Considering that the reddest and most massive galaxies have been formed earlier (at $z > 2$, having already an age of >1 Gyr at $z \sim 1$, see e.g. Vergani et al. 2008 and references therein), and that moreover their Star Formation Histories (SFH) are typically faster ($\lesssim$3 Gyr, see e.g. Gavazzi et al. 2002) than those of lower mass galaxies, their formation epoch and their evolution time-scale took place on the mean before an appreciable growth of structures (at $z \sim 1$ the number of structures with $\log(M/M_\odot) > 5 \times 10^{14}$ was ~100 times lower than today, in the concordance cosmology, see Borgani 2006). We do not see evident environmental effects on these galaxies because environment could not affect their evolution. On the contrary, lower mass galaxies ($\log(M/M_\odot) \lesssim 10.7$) not only have been formed more recently, but their SFH are also slower. Therefore, physical processes typical of high density regions could have modified their SFH itself. For a broad picture about the role of mass and

environment in driving galaxy evolution, obtained with SDSS and zCOSMOS data, we refer the reader to Peng et al. (2010).

This picture is in agreement with the scenario that has been already proposed in literature where both "nature" and "nurture" affect galaxy properties (see e.g. Kauffmann et al. 2004; De Lucia et al. 2006; Cucciati et al. 2006), to which we can add the dependence on mass. First, galaxy formation is "biased" (Marinoni et al. 2005), meaning that more massive galaxies formed first in the highest density peaks, later on followed by lower mass galaxies in less dense environment. Second, for relatively low mass galaxies the evolution is affected by complex physical processes that depend on the local environment. According to this picture, the properties of a low-mass galaxy are thus affected by the environment in which the galaxy resides at any given epoch of its evolution, and not only at the time of its formation, as a simple imprinting.

Unfortunately, the relatively large uncertainties in our measurements prevent us from assessing in a precise and quantitative way the relative roles that "nature" and "nurture" did play. We defer this study to a future work.

10. Summary and conclusions

In this work we use the first ∼10 000 spectra of the purely flux limited zCOSMOS *bright* sample ($I_{\rm AB} \leq 22.5$) to investigate the redshift evolution of environmental effects on galaxy spectro-photometric properties, mainly $U-B$ colour, in the range $0.1 \leq z \leq 1.0$. We refer the reader to Kovač et al. (2010a) for a full description of the environment parametrization via the local density field. More in details, we want to disentangle the multiple dependence among local density, galaxy colour and stellar mass, in order to verify whether the environment acts directly on both stellar mass and colour, that are related to each other. Our main results are the following.

- Using a luminosity-selected volume-limited sample ($M_B \leq -20.5 - z$) we find, confirming previous results, that the fraction of red ($U - B \geq 1$) galaxies depends on environment at least up to $z \sim 1$, with red galaxies residing preferentially in high density environments. This trend becomes weaker for higher redshifts, and it is mirrored by the one we observe for the fraction of galaxies with $D_n4000 \geq 1.4$. We also find that the fraction of galaxies with $\log(EW[\mathrm{OII}]) \geq 1.15$ is higher for lower densities, and this is true up to $z \sim 1$. Also in this case we observe a weakening of the environmental effects for increasing redshift.
- Given the fact that stellar mass depends on local density (see e.g. Bolzonella et al. 2010 and our Fig. 7), and given that colour depends on mass, it is difficult to interpret the meaning of the colour-density relation in a luminosity-selected sample. In fact, the wide spread in mass-to-light ratios embedded in this selection leave us with a broad range in stellar masses, that biases any possible direct colour-density relation via the mass segregation as a function of environment.
- We disentangle the colour-mass-density relation using galaxy subsamples enclosed in narrow mass bins, to avoid any dependence of mass on local density. We study the colour-density relation in mass bins of $\Delta \log(M/M_\odot) = 0.2$, in three different redshift bins within the range 0.1–1.0, paying attention to attain to the mass limits imposed by the flux limit of our survey. We find that, once the mass is fixed, the colour-density relation is globally flat, but with some exceptions. We observe that within $0.1 \leq z \leq 0.5$ the fraction of "very red" galaxies depends on environment even when mass is fixed, at least for $\log(M/M_\odot) \lesssim 10.7$ (see Sect. 6.2 for the definition of "very red" galaxies). This means that environment affects directly not only the stellar mass, but also other galaxy properties, at least for these given mass and redshift ranges.

According to these results, we suggest a scenario in which the colour depends primarily on mass, but for a relatively low-mass regime ($10.2 \lesssim \log(M/M_\odot) \lesssim 10.7$) the local environment modulates this dependence. These galaxies have been formed more recently, in an epoch where evolved structures were already in place. Moreover, the physical processes typical of high density regions could operate during longer periods of time in shaping the properties of these galaxies, thanks to their longer (on average) star formation histories.

It is not possible with this analysis to quantitatively assess the relative role of biased initial conditions (more massive galaxies form first and in more dense environments) and of physical processes acting during galaxies lifetimes, in order to precisely explain the origin (or the absence) of both colour- and mass-density relations. We refer the reader to Peng et al. (2010) for a more comprehensive analysis on how mass and environment affect galaxy evolution. On the one hand, the forthcoming zCOSMOS 20*k* bright survey will allow us a more detailed analysis of these mass and redshift regimes, on the other hand this work has to be complemented by the study of the redshift evolution of the less massive galaxies population, that is not possible within the zCOSMOS bright sample, and that is of crucial importance to better understand how environment affects the different galaxy populations.

Acknowledgements. We thank the referee for helpful comments. This work has been supported in part by the grant ASI/COFIS/WP3110 I/026/07/0.

References

Baldry, I. K., Glazebrook, K., Brinkmann, J., et al. 2004, ApJ, 600, 681
Baldry, I. K., Balogh, M. L., Bower, R. G., et al. 2006, MNRAS, 373, 469
Balogh, M. L., Morris, S. L., Yee, H. K. C., Carlberg, R. G., & Ellingson, E. 1999, ApJ, 527, 54
Balogh, M. L., Baldry, I. K., Nichol, R., et al. 2004, ApJ, 615, L101
Bell, E. F., Wolf, C., Meisenheimer, K., et al. 2004, ApJ, 608, 752
Blanton, M. R., Eisenstein, D., Hogg, D. W., Schlegel, D. J., & Brinkmann, J. 2005, ApJ, 629, 143
Blanton, M. R., Eisenstein, D., Hogg, D. W., & Zehavi, I. 2006, ApJ, 645, 977
Bolzonella, M., Miralles, J.-M., & Pelló, R. 2000, A&A, 363, 476
Bolzonella, M., Kovac, K., Pozzetti, L., et al. 2010, A&A, in press [arXiv:0907.0013]
Borgani, S. 2006, unpublished [astro-ph/0605575]
Boselli, A., & Gavazzi, G. 2006, PASP, 118, 517
Brinchmann, J., Charlot, S., White, S. D. M., et al. 2004, MNRAS, 351, 1151
Bruzual A., G., & Charlot, S. 1993, ApJ, 405, 538
Bruzual, G., & Charlot, S. 2003, MNRAS, 344, 1000
Bundy, K., Ellis, R. S., Conselice, C. J., et al. 2006, ApJ, 651, 120
Calzetti, D., Armus, L., Bohlin, R. C., et al. 2000, ApJ, 533, 682
Capak, P., Aussel, H., Ajiki, M., et al. 2007, ApJS, 172, 99
Caputi, K. I., Kovač, K., Bolzonella, M., et al. 2009, ApJ, 691, 91
Chabrier, G. 2003, PASP, 115, 763
Coil, A. L., Davis, M., Madgwick, D. S., et al. 2004a, ApJ, 609, 525
Coil, A. L., Newman, J. A., Kaiser, N., et al. 2004b, ApJ, 617, 765
Coleman, G. D., Wu, C., & Weedman, D. W. 1980, ApJS, 43, 393
Colless, M., Dalton, G., Maddox, S., et al. 2001, MNRAS, 328, 1039
Cooper, M. C., Newman, J. A., Croton, D. J., et al. 2006, MNRAS, 370, 198
Cooper, M. C., Newman, J. A., Coil, A. L., et al. 2007, MNRAS, 376, 1445
Cooper, M. C., Newman, J. A., Weiner, B. J., et al. 2008, MNRAS, 383, 1058
Croton, D. J., Farrar, G. R., Norberg, P., et al. 2005, MNRAS, 356, 1155
Cucciati, O., Iovino, A., Marinoni, C., et al. 2006, A&A, 458, 39
Cucciati, O., Marinoni, C., Iovino, A., et al. 2010, A&A, 520, A42
Davis, M., Faber, S. M., Newman, J., et al. 2003, in Discoveries and Research Prospects from 6- to 10-Meter-Class Telescopes II. Puragra. Proceedings of the SPIE, ed. P. Guhathakurta, 4834, 161

De Lucia, G., Springel, V., White, S. D. M., Croton, D., & Kauffmann, G. 2006, MNRAS, 366, 499
De Propris, R., Colless, M., Peacock, J. A., et al. 2004, MNRAS, 351, 125
Djorgovski, S., & Davis, M. 1987, ApJ, 313, 59
Dressler, A. 1980, ApJ, 236, 351
Dressler, A., Lynden-Bell, D., Burstein, D., et al. 1987, ApJ, 313, 42
Dressler, A., Oemler, A. J., Couch, W. J., et al. 1997, ApJ, 490, 577
Elbaz, D., Daddi, E., Le Borgne, D., et al. 2007, A&A, 468, 33
Fasano, G., Poggianti, B. M., Couch, W. J., et al. 2000, ApJ, 542, 673
Feldmann, R., Carollo, C. M., Porciani, C., et al. 2006, MNRAS, 372, 565
Finoguenov, A., Guzzo, L., Hasinger, G., et al. 2007, ApJS, 172, 182
Fioc, M., & Rocca-Volmerange, B. 1997, A&A, 326, 950
Franzetti, P., Scodeggio, M., Garilli, B., et al. 2007, A&A, 465, 711
Gavazzi, G., Pierini, D., & Boselli, A. 1996, A&A, 312, 397
Gavazzi, G., & Scodeggio, M. 1996, A&A, 312, L29
Gavazzi, G., Bonfanti, C., Sanvito, G., Boselli, A., & Scodeggio, M. 2002, ApJ, 576, 135
Gehrels, N. 1986, ApJ, 303, 336
Gunn, J. E., & Gott, J. R. I. 1972, ApJ, 176, 1
Hogg, D. W., Blanton, M. R., Brinchmann, J., et al. 2004, ApJ, 601, L29
Hubble, E. P. 1926, ApJ, 64, 321
Ilbert, O., Tresse, L., Zucca, E., et al. 2005, A&A, 439, 863
Ilbert, O., Cucciati, O., Marinoni, C., et al. 2006, unpublished [astro-ph/0602329]
Iovino, A., Cucciati, O., Scodeggio, M., et al. 2010, A&A, 509, A40
Kauffmann, G., Heckman, T. M., White, S. D. M., et al. 2003, MNRAS, 341, 54
Kauffmann, G., White, S. D. M., Heckman, T. M., et al. 2004, MNRAS, 353, 713
Kinney, A. L., Calzetti, D., Bohlin, R. C., et al. 1996, ApJ, 467, 38
Knobel, C., Lilly, S. J., Iovino, A., et al. 2009, ApJ, 697, 1842
Koekemoer, A. M., Aussel, H., Calzetti, D., et al. 2007, ApJS, 172, 196
Kovac, K., Porciani, C., Lilly, S. J., et al. 2009, ApJ, submitted [arXiv:0910.0004]
Kovač, K., Lilly, S. J., Cucciati, O., et al. 2010a, ApJ, 708, 505
Kovač, K., Lilly, S. J., Knobel, C., et al. 2010b, ApJ, 718, 86
Lamareille, F., Contini, T., Le Borgne, J., et al. 2006, A&A, 448, 893
Larson, R. B., Tinsley, B. M., & Caldwell, C. N. 1980, ApJ, 237, 692
Le Borgne, J.-F., Bruzual, G., Pelló, R., et al. 2003, A&A, 402, 433
Le Fèvre, O., Saisse, M., Mancini, D., et al. 2003, in Instrument Design and Performance for Optical/Infrared Ground-based Telescopes. ed. M. Iye, A. F. M. Moorwood, Proceedings of the SPIE, 4841, 1670
Le Fèvre, O., Vettolani, G., Garilli, B., et al. 2005, A&A, 439, 845
Lilly, S. J., Le Fèvre, O., Renzini, A., et al. 2007, ApJS, 172, 70
Lilly, S. J., Le Brun, V., Maier, C., et al. 2009, ApJS, 184, 218
Madgwick, D. S., Hawkins, E., Lahav, O., et al. 2003, MNRAS, 344, 847
Maier, C., Lilly, S. J., Zamorani, G., et al. 2009, ApJ, 694, 1099
Mandelbaum, R., Seljak, U., Kauffmann, G., Hirata, C. M., & Brinkmann, J. 2006, MNRAS, 368, 715
Maraston, C. 2005, MNRAS, 362, 799
Marinoni, C., Le Fèvre, O., Meneux, B., et al. 2005, A&A, 442, 801
Menanteau, F., Ford, H. C., Motta, V., et al. 2006, AJ, 131, 208
Meneux, B., Le Fèvre, O., Guzzo, L., et al. 2006, A&A, 452, 387
Meneux, B., Guzzo, L., Garilli, B., et al. 2008, A&A, 478, 299
Meneux, B., Guzzo, L., de La Torre, S., et al. 2009, A&A, 505, 463
Moore, B., Katz, N., Lake, G., Dressler, A., & Oemler, A. 1996, Nature, 379, 613
Norberg, P., Baugh, C. M., Hawkins, E., et al. 2002, MNRAS, 332, 827
Oemler, A. J. 1974, ApJ, 194, 1
Oesch et al. 2010, ApJL, submitted [arXiv:1005.1661]
Peng, Y., Lilly, S. J., Kovač, K., et al. 2010, ApJ, 721, 193
Poggianti, B. M., von der Linden, A., De Lucia, G., et al. 2006, ApJ, 642, 188
Pollo, A., Guzzo, L., Le Fèvre, O., et al. 2006, A&A, 451, 409
Postman, M., Franx, M., Cross, N. J. G., et al. 2005, ApJ, 623, 721
Pozzetti, L., Bolzonella, M., Lamareille, F., et al. 2007, A&A, 474, 443
Pozzetti, L., Bolzonella, M., Zucca, E., et al. 2010, A&A, 523, A13
Sandage, A. 1975, Galaxies and the Universe, ed. A. Sandage, M. Sandage, & J. Kristien (Chicago: Univ.Chicago Press)
Scodeggio, M., Gavazzi, G., Franzetti, P., et al. 2002, A&A, 384, 812
Scodeggio, M., Vergani, D., Cucciati, O., et al. 2009, A&A, 501, 21
Scoville, N., Aussel, H., Benson, A., et al. 2007a, ApJS, 172, 150
Scoville, N., Aussel, H., Brusa, M., et al. 2007b, ApJS, 172, 1
Silverman, J. D., Kovač, K., Knobel, C., et al. 2009a, ApJ, 695, 171
Silverman, J. D., Lamareille, F., Maier, C., et al. 2009b, ApJ, 696, 396
Smith, G. P., Treu, T., Ellis, R. S., Moran, S. M., & Dressler, A. 2005, ApJ, 620, 78
Tanaka, M., Goto, T., Okamura, S., Shimasaku, K., & Brinkmann, J. 2004, AJ, 128, 2677
Tasca, L. A. M., Kneib, J., Iovino, A., et al. 2009, A&A, 503, 379
Toomre, A., & Toomre, J. 1972, ApJ, 178, 623
Tremonti, C. A., Heckman, T. M., Kauffmann, G., et al. 2004, ApJ, 613, 898
Treu, T., Ellis, R. S., Kneib, J.-P., et al. 2003, ApJ, 591, 53
Tully, R. B., Mould, J. R., & Aaronson, M. 1982, ApJ, 257, 527
Vergani, D., Scodeggio, M., Pozzetti, L., et al. 2008, A&A, 487, 89
Visvanathan, N., & Sandage, A. 1977, ApJ, 216, 214
Willmer, C. N. A., Faber, S. M., Koo, D. C., et al. 2006, ApJ, 647, 853
Yang, X., Mo, H. J., & van den Bosch, F. C. 2008, ApJ, 676, 248
York, D. G., Adelman, J., Anderson, Jr., J. E., et al. 2000, AJ, 120, 1579
Zehavi, I., Blanton, M. R., Frieman, J. A., et al. 2002, ApJ, 571, 172
Zucca, E., Ilbert, O., Bardelli, S., et al. 2006, A&A, 455, 879
Zucca, E., Bardelli, S., Bolzonella, M., et al. 2009, A&A, 508, 1217

[1] Laboratoire d'Astrophysique de Marseille, UMR 6110 CNRS-Université de Provence, 38 rue Frederic Joliot-Curie, 13388 Marseille Cedex 13, France
e-mail: olga.cucciati@oamp.fr
[2] INAF-Osservatorio Astronomico di Brera, via Brera 28, 20121 Milano, Italy
[3] Institute of Astronomy, ETH Zürich, 8093 Zürich, Switzerland
[4] INAF – IASF, via Bassini 15, 20133 Milano, Italy
[5] INAF – Osservatorio Astronomico di Bologna, via Ranzani 1, 40127 Bologna, Italy
[6] Laboratoire d'Astrophysique de Toulouse-Tarbes, Université de Toulouse, CNRS, 14 avenue Edouard Belin, 31400 Toulouse, France
[7] European Southern Observatory, Karl-Schwarzschild-Strasse 2, Garching 85748, Germany
[8] INAF – Osservatorio Astronomico di Padova, Padova, Italy
[9] Max-Planck-Institut für extraterrestrische Physik, 84571 Garching, Germany
[10] Dipartimento di Astronomia, Universitá di Bologna, via Ranzani 1, 40127 Bologna, Italy
[11] INAF – Osservatorio Astronomico di Brera, via Bianchi 46, 23807 Merate (LC), Italy
[12] Instituto de Astrofísica de Andalucía - CSIC. Apdo. de correos 3004, 18080 Granada, Spain
[13] Dipartimento di Astronomia, Universitá di Padova, vicolo Osservatorio 3, 35122 Padova, Italy
[14] Space Telescope Science Institute, 3700 San Martin Drive, Baltimore, MD 21218, USA
[15] California Institute of Technology, MS 105-24, Pasadena, CA 91125, USA
[16] INAF – Osservatorio Astronomico di Torino, Strada Osservatorio 20, 10025 Pino Torinese, Italy
[17] Dept. of Astronomy, University of Massachusetts at Amherst
[18] Physics Division, MS 50 R5004, Lawrence Berkeley National Laboratory, 1 Cyclotron Rd., Berkeley, CA 94720, USA
[19] Centre de Physique Théorique, UMR 6207 CNRS-Université de Provence, 13288 Marseille, France
[20] Institut d'Astrophysique de Paris, UMR 7095 CNRS, Université Pierre et Marie Curie, 98 bis Boulevard Arago, 75014 Paris, France
[21] Universitats-Sternwarte, Scheinerstrasse 1, 81679 Muenchen, Germany
[22] Argelander Institut für Astronomie, Auf dem Hügel 71, 53121 Bonn, Germany
[23] INAF, Osservatorio di Roma, Monteporzio Catone (RM), Italy